

1 **Quantitative H₂S-mediated protein sulfhydration reveals metabolic**
2 **reprogramming during the Integrated Stress Response**

3

4 Xing-Huang Gao¹, Dawid Krokowski¹, Bo-Jhih Guan^{1#}, Ilya Bederman^{2#}, Mithu
5 Majumder¹⁰, Marc Parisien³, Luda Diatchenko³, Omer Kabil⁴, Belinda Willard⁵,
6 Ruma Banerjee⁴, Benlian Wang⁶, Gurkan Bebek⁶, Charles R Evans⁷, Paul L.
7 Fox⁸, Stanton L Gerson⁹, Charles L. Hoppel¹⁰, Ming Liu⁷, Peter Arvan⁷, and Maria
8 Hatzoglou^{1*}

9

10 **Author affiliations**

11 ¹Case Western Reserve University, Department of Genetics and Genome
12 Sciences, Cleveland, OH, USA

13 ²Case Western Reserve University, Department of Pediatrics, Cleveland, OH,
14 USA

15 ³McGill University, Alan Edwards Centre for Research on Pain, Montreal, QC,
16 Canada

17 ⁴University of Michigan Medical School, Biological Chemistry, Ann Arbor, MI,
18 USA

19 ⁵Lerner Research Institute, Mass Spectrometry Laboratory for Protein
20 Sequencing, Cleveland Clinic, Cleveland, OH, USA

21 ⁶ Case Western Reserve University, Center for Proteomics and Bioinformatics,
22 Center for Synchrotron Biosciences, School of Medicine, Cleveland, Ohio, USA

23 ⁷University of Michigan Medical School, Department of Internal Medicine,
24 Division of Metabolism, Endocrinology & Diabetes, Ann Arbor, MI, USA

25 ⁸Lerner Research Institute, Department of Cellular and Molecular Medicine,
26 Cleveland Clinic, Cleveland, OH, USA

27 ⁹Case Western Reserve University, Department of Medicine, Division of
28 Hematology/Oncology, School of Medicine, 2103 Cornell Road, Cleveland, OH,
29 USA

30 ¹⁰Case Western Reserve University, Department of Pharmacology, Cleveland,
31 OH, USA

32 # Equally contributing authors

33 *Corresponding author. E-mail: mxh8@case.edu

34

35 **Abstract**

36 The sulfhydration of cysteine residues in proteins is an important mechanism
37 involved in diverse biological processes. We have developed a proteomics
38 approach to quantitatively profile the changes of sulfhydrated cysteines in
39 biological systems. Bioinformatics analysis revealed that sulfhydrated cysteines
40 are part of a wide range of biological functions. In pancreatic β cells exposed to
41 endoplasmic reticulum (ER) stress, elevated H_2S promotes the sulfhydration of
42 enzymes in energy metabolism and stimulates glycolytic flux. We propose that
43 transcriptional and translational reprogramming by the Integrated Stress
44 Response (ISR) in pancreatic β cells is coupled to metabolic alternations
45 triggered by sulfhydration of key enzymes in intermediary metabolism.

46

47

48 **Introduction**

49 Posttranslational modification is a fundamental mechanism in the regulation of
50 structure and function of proteins. The covalent modification of specific amino
51 acid residues influences diverse biological processes and cell physiology across
52 species. Reactive cysteine residues in proteins have high nucleophilicity and low
53 pKa values and serve as a major target for oxidative modifications, which can
54 vary depending on the subcellular environment, including the type and intensity
55 of intracellular or environmental cues. Oxidative environments cause different
56 post-translational cysteine modifications, including disulfide bond formation (-S-
57 S-), sulfenylation (-S-OH), nitrosylation (-S-NO), glutathionylation (-S-SG), and
58 sulfhydrylation (-S-SH) (also called persulfidation) (Finkel, 2012; Mishanina et al.,
59 2015). In the latter, an oxidized cysteine residue included glutathionylated,
60 sulfenylated and nitrosylated on a protein reacts with the sulfide anion to form a
61 cysteine persulfide. The reversible nature of this modification provides a
62 mechanism to fine tune biological processes in different cellular redox states.
63 Sulfhydrylation coordinates with other post-translational protein modifications such
64 as phosphorylation and nitrosylation to regulate cellular functions (Altaany et al.,
65 2014; Sen et al., 2012). Despite great progress in bioinformatics and advanced
66 mass spectroscopic techniques (MS), identification of different cysteine-based
67 protein modifications has been slow compared to other post-translational
68 modifications. In the case of sulfhydrylation, a small number of proteins have been
69 identified, among them the glycolytic enzyme glyceraldehyde phosphate
70 dehydrogenase, GAPDH (Mustafa et al., 2009). Sulfhydrated GAPDH at Cys¹⁵⁰

71 exhibits an increase in its catalytic activity, in contrast to the inhibitory effects of
72 nitrosylation or glutathionylation of the same cysteine residue (Mustafa et al.,
73 2009; Paul and Snyder, 2012). The biological significance of the Cys¹⁵⁰
74 modification by H₂S is not well-studied, but H₂S could serve as a biological switch
75 for protein function acting via oxidative modification of specific cysteine residues
76 in response to redox homeostasis (Paul and Snyder, 2012). Understanding the
77 physiological significance of protein sulfhydration requires the development of
78 genome-wide innovative experimental approaches. Current methodologies based
79 on the modified biotin switch technique do not allow detection of a broad
80 spectrum of sulfhydrated proteins (Finkel, 2012). Guided by a previously reported
81 strategy (Sen et al., 2012), we developed an experimental approach that allowed
82 us to quantitatively evaluate the sulfhydrated proteome and the physiological
83 consequences of H₂S synthesis during chronic ER stress. The new methodology
84 allows a quantitative, close-up view of the integrated cellular response to
85 environmental and intracellular cues, and is pertinent to our understanding of
86 human disease development.

87 The ER is an organelle involved in synthesis of proteins followed by various
88 modifications. Disruption of this process results in the accumulation of misfolded
89 proteins, causing ER stress (Tabas and Ron, 2011; Walter and Ron, 2011),
90 which is associated with development of many diseases ranging from metabolic
91 dysfunction to neurodegeneration (Hetz, 2012). ER stress induces
92 transcriptional, translational, and metabolic reprogramming, all of which are
93 interconnected through the transcription factor Atf4. Atf4 increases expression of

94 genes promoting adaptation to stress via their protein products. One such gene
95 is the H₂S-producing enzyme, γ -cystathionase (CTH), previously shown to be
96 involved in the signaling pathway that negatively regulates the activity of the
97 protein tyrosine phosphatase 1B (PTP1B) via sulfhydration (Krishnan et al.,
98 2011). We therefore hypothesized that low or even modest levels of reactive
99 oxygen species (ROS) during ER stress may reprogram cellular metabolism via
100 H₂S-mediated protein sulfhydration (Figure 1A).

101

102 **Results**

103 We have previously shown that the insulin-producing mouse pancreatic β cells
104 MIN6, known for their high metabolic activity, are very susceptible to ER stress
105 (Guan et al., 2014; Krokowski et al., 2013a). We tested whether or not MIN6 cells
106 expressed the essential components of H₂S synthesis and protein sulfhydration
107 in response to ER stress induced by thapsigargin (Tg, Figure 1). Upon Tg
108 treatment, MIN6 cells exhibited higher levels of intracellular ROS, decreased
109 GSH/GSSG ratios, and increased CTH protein levels via transcriptional activation
110 (Figure 1B-D, Figure 1-figure supplement 1 and 2A). This transcriptional
111 reprogramming also was seen in mouse and human islets subjected to
112 physiological or pharmacologically-induced ER stress (Figure 1D, Figure 1-figure
113 supplement 2B-C and 3). In agreement with increased CTH expression, H₂S
114 levels increased during the chronic phase of the stress response (Figure 1E).
115 Coordinated induction of expression of the gene encoding the glutamate/cystine
116 exchanger, Slc7a11, also was increased (Figure 1D), and this induction was

117 associated with increased glutamate/cystine flux (Figure 1- figure supplement 4).
118 Slc7a11 mediates the exchange of oxidized extracellular cystine with intracellular
119 glutamate. Once cystine is imported into the cells it gets reduced to cysteine,
120 then serves as a substrate for GSH and H₂S synthesis. These data support the
121 idea that both increased uptake of the CTH substrate (cysteine) and increased
122 levels of CTH contribute to increased H₂S levels in cells under ER stress.

123 The functional significance of increased H₂S synthesis was shown by measuring
124 the catalytic activity of GAPDH (Mustafa et al., 2009), which gradually increased
125 in response to elevated H₂S production in MIN6 cells during ER stress (Figure
126 1F). This increase in activity was independent of GAPDH protein levels (Figure
127 1F). As noted above, GAPDH has the unusual feature of being catalytically
128 inactive when Cys¹⁵⁰ is oxidatively modified, except when it undergoes
129 sulfhydration which restores/increases its activity (Mustafa et al., 2009). We
130 therefore tested the protective effects of Cys¹⁵⁰ sulfhydration by H₂S on its
131 catalytic activity in the presence of H₂O₂-induced oxidation. Recombinant
132 GAPDH was incubated with H₂O₂ in the presence or absence of the H₂S donor,
133 NaHS. The inhibition of GAPDH activity by H₂O₂ was significantly reversed by
134 H₂S treatment (Figure 1G). Furthermore, incubation of purified GAPDH with
135 oxidized glutathione (GSSG) resulted in formation of inactive glutathionylated
136 GAPDH (Gao et al., 2010), which was significantly rescued by treatment with H₂S
137 as well as DTT reduction (Figure 1H). HPLC-MS confirmed that recombinant
138 GAPDH exposed to NaHS or GSSG was modified predominantly at Cys¹⁵⁰
139 (Figure 1-figure supplement 5, Figure 2-figure supplement 7B-C). These data

140 confirm that H₂S is a positive regulator of GAPDH activity. Increased GAPDH
141 activity is directly linked to H₂S production, as shown by the loss of induction
142 (Figure 1I) upon treatment with the CTH inhibitor, propargylglycine (PAG). PAG
143 inhibits H₂S synthesis and therefore is expected to decrease Cys¹⁵⁰ modification.
144 Taken together, these results indicate that regulation of H₂S synthesis during ER
145 stress might regulate the catalytic activity of other metabolic pathway proteins.
146 The latter is raising the possibility that the ATF4-mediated sulfhydration of
147 proteins is part of the Integrated Stress Response (ISR), and has regulatory
148 effects on cellular metabolism.

149 Atf4 increases gene expression of CTH (Dickhout et al., 2012), the cystine
150 transporter Slc7a11, as well as the ROS-producing enzyme Ero1 α (Han et al.,
151 2013; Tabas and Ron, 2011). We hypothesized that during ER stress this
152 network of ATF4 target genes promotes protein sulfhydration (Figure 2A).
153 Knockdown of ATF4 in MIN6 cells during Tg-induced ER stress caused inhibition
154 of H₂S synthesis with a parallel loss of induction of CTH protein levels (Figure
155 2B). In contrast, in the absence of stress, ATF4 overexpression increased CTH
156 and Ero1 α levels and H₂S synthesis, in agreement with increased GAPDH
157 activity (Figure 2C-E, Figure 2-figure supplement 1). The levels of GSH and the
158 activity of the glutamate/cystine exchanger also increased with ATF4
159 overexpression (Figure 2F-G). These data support the hypothesis that ATF4 is a
160 master regulator of protein sulfhydration in pancreatic β cells during ER stress.

161 To profile genome-wide changes in protein sulfhydration by ER stress and the
162 integrated stress response, we exploited the different reactivity of cysteine

163 persulfides (Cys-S-SH) and thiols (Cys-SH) to alkylating agents (Nishida et al.,
164 2012; Pan and Carroll, 2013; Paul and Snyder, 2012), to develop a new thiol
165 reactivity-based approach called BTA (Biotin Thiol Assay, (Figure 2H and Figure
166 2-figure supplement 2). We employed the following steps (Figure 2H): (1)
167 labeling of reactive Cys-SH or Cys-S-SH groups by a biotin-conjugated
168 maleimide (maleimide-PEG2-biotin, NM-biotin) (Weerapana et al., 2010), (2)
169 binding of the biotin-labeled proteins on an avidin column, (3) elution of the
170 retained proteins that contain a persulfide bridge using DTT and (4) analysis of
171 the eluted proteins.

172 The BTA approach was validated by testing the hypothesis that a lower
173 concentration of the thiol-alkylating reagent (NM-biotin) will result in a selective
174 labeling of highly reactive cysteine SH groups, and that this selectivity will be lost
175 as the concentration of NM-biotin increases (Weerapana et al., 2010). We tested
176 this hypothesis in extracts isolated from Tg-treated MIN6 cells in the presence of
177 increasing concentrations of NM-biotin (0.05 to 1 mM). The eluate containing the
178 sulfhydrated proteins was analyzed with SDS-PAGE and the proteins were
179 visualized by Coomassie blue staining. Indeed, increasing the concentration of
180 NM-biotin beyond 0.5 mM decreased the levels of eluted proteins (Figure 2-figure
181 supplement 3), consistent with cysteine residues having free -SH groups
182 becoming alkylated at high concentrations of NM-biotin. No protein was eluted
183 from the column with the addition of DTT at high concentrations of NM-biotin
184 (Figure 2-figure supplement 3), confirming that the biotin was attached to
185 proteins via a disulfide bond (Figure 2-figure supplement 4A). This selectively

186 labeling behavior not only relies on the probe concentration, but also is
187 dependent on the protein structure conformations. We found that no protein was
188 detected in the eluates if the BTA was performed on the denatured cell extracts
189 (data not shown).

190 When Tg-treated MIN6 lysates were pretreated with DTT (to decrease the level
191 of sulfhydrated proteins), the signal was significantly reduced compared to
192 untreated lysates (Figure 2-figure supplement 4B), confirming that DTT reduces
193 an intermolecular disulfide bond of cysteine persulfides labeled with biotin. These
194 data show that sulfhydrated cysteine residues are the primary targets of NM-
195 biotin at low concentrations, thus making the BTA a unique tool to identify the
196 sulfhydrated proteome (Figure 2-figure supplement 2).

197 We next assessed the BTA assay using recombinant GAPDH, which contains six
198 cysteine residues including the redox-regulated Cys¹⁵⁰. GAPDH was incubated
199 with either H₂O₂ or NaHS. The presence of sulfhydrated GAPDH was evaluated
200 by the BTA method following Western blot analysis. We found that only the
201 NaHS-treated GAPDH was eluted as an H₂S-modified target, indicating that the
202 assay distinguishes sulfhydration or free SH groups from other forms of cysteine
203 modifications (Figure 2-figure supplement 5B). This was independently confirmed
204 with the red maleimide assay (Figure 2-figure supplement 6), which discriminates
205 between free -SH groups and sulfhydrated-SH (Sen et al., 2012). We next tested
206 if the BTA can identify modification of a specific cysteine on GAPDH by using
207 recombinant wild-type and Cys¹⁵⁰Ser GAPDH mutant, which were incubated with
208 H₂O₂ or NaHS. We found that NaHS treatment induced sulfhydration in the wild-

209 type GAPDH (Figure 2-figure supplement 7A), a result that was also confirmed
210 by high-resolution quadruple MS analysis (Figure 2-figure supplement 7B-C), and
211 that this modification was absent in the Cys¹⁵⁰Ser mutant. Finally, a proteome-
212 wide view of sulfhydration was obtained from Tg-treated MIN6 cell extracts
213 subjected to BTA and further analyzed by LC-MS/MS (Figure 2-figure
214 supplement 8). We identified 150 proteins, including several known targets for
215 sulfhydration (Figure 2-figure supplement 8D) (Mustafa et al., 2009). Similar
216 results were obtained from analysis of mouse liver (data not shown), a tissue
217 known to exhibit high levels of H₂S synthesis (Kabil et al., 2011). Taken together,
218 this shows that BTA discriminates between protein sulfhydration and other
219 oxidative modifications.

220 Next, the BTA methodology identified the sulfhydrated proteome downstream of
221 the transcription factor Atf4 during ER stress (Figure 2A). MIN6 cells treated with
222 Tg increased GAPDH levels in the DTT eluate, that was abolished by knocking
223 down *Atf4* (Figure 2I). In the absence of stress, ATF4 knockdown resulted in an
224 increase in sulfhydrated GAPDH in MIN6 cells (Figure 2I). Because ATF4-
225 deficient cells have decreased levels of sulfur-containing amino acids (Harding et
226 al., 2003), and sulfur amino acid restriction is linked to an increase in the
227 transulfuration pathway (Hine et al., 2015), it is possible that the increase in
228 GAPDH sulfhydration in ATF4-depleted cells is due to activation of CBS (Niu et
229 al., 2015), the second cytosolic H₂S-producing enzyme. Moreover, we found that
230 in the absence of stress ATF4 overexpression induced GAPDH sulfhydration that
231 is dependent on the CTH activity (Figure 2J-K). The use of PAG decreased

232 GAPDH sulfhydration (Figure 2K). We conclude that sulfhydration of proteins
233 during ER stress is part of the ISR and is controlled by the transcription factor,
234 Atf4.

235 The BTA requires determining the concentration of NM-Biotin for selectively
236 labeling proteins with reactive, sulfhydrated cysteines rather than the relatively
237 high abundant and less reactive, unmodified (with free SH groups) cysteine
238 residues. However, this labeling step has some limitations under certain
239 circumstances. For example, if free Cys-SH groups are biotinylated on the same
240 protein containing one or more Cys-S-SH groups (Figure 2H and Figure 2-figure
241 supplement 2), then the protein will not be eluted with DTT and will not be
242 identified as a target for sulfhydration. In addition, if a protein contains
243 sulfhydrated cysteines with low reactivity for the probe, this protein will not be
244 captured and identified as an H₂S-modified target. Due to those limitations and
245 in order to extend the capability of the BTA approach, we introduced a proteolytic
246 digestion step before applying the avidin column step. This added step provided
247 not only the isolation of cysteine-containing peptides with persulfide bonds, but
248 also increased the identification of sulfhydrated proteins. The eluted peptides
249 were then sequenced and identified by LC-MS/MS analysis, thereby identifying
250 the modified cysteines on proteins. By using the modified BTA technique, we
251 have identified over ~ 1,000 novel sulfhydrated cysteines in MIN6 cells treated
252 with Tg, corresponding to about 820 proteins (Figure 2- figure supplement 9 and
253 source data 1), including GAPDH, wherein two cysteine-containing peptides were
254 captured: Cys¹⁵⁰ and Cys²⁴⁵. Remarkably, the Cys¹⁵⁰ active-site peptide was

255 highly enriched as compared to the C-terminal of Cys²⁴⁵, supporting prior
256 mutagenesis studies that have shown Cys¹⁵⁰ as the primary H₂S-modified site on
257 GAPDH, both in vitro and in vivo. One of novel targets including
258 phosphoglycerate dehydrogenase (PHGDH) was also confirmed by Western blot
259 analysis (Figure 2- figure supplement 10). CTH Knockdown mediated by shRNA
260 decreased GAPDH and PHGDH sulfhydrylation levels, confirming that those
261 proteins identified by the BTA method are bona-fide targets for sulfhydrylation in
262 vivo (Figure 3-figure supplement 11). Finally, there is no correlation between
263 protein abundance and sulfhydrylation (Figure 3-figure supplement 6-7 and source
264 data 2), supporting that lower concentrations of the NM-biotin labeling reveal
265 reactivity of cysteine residues rather than protein abundance.

266 In order to obtain genome-wide stress-induced changes in the sulfhydrylation and
267 individual cysteine residues within these proteins, we devised a modified BTA
268 protocol (Figure 3A) by introducing a stable isotope-labeling step after the DTT
269 elution step. This protocol uses (1) digestion of biotinylated cell extracts with
270 trypsin before avidin capture, (2) labeling of free Cys-SH groups on peptides in
271 the column eluent by mass-difference cysteine-alkylating reagents with either
272 NEM-H₅ (Light) or NEM-D₅ (Heavy) and (3) quantification by LC-MS/MS analysis
273 of H/L ratios of the individual pair-labeled cysteines in the identified peptides
274 based on a mass-difference labeling. In addition to quantifying changes in protein
275 sulfhydrylation, this modified BTA approach allows the detection of additional
276 proteins. We used as an experimental system the ATF4-expressing MIN6 cells to
277 profile quantitatively the sulfhydrylated proteome. As shown in Figure 2A, ATF4-

278 mediated signaling triggers the cellular response, which leads to increased
279 protein sulfhydration. Using the experimental plan in Figure 3A, we identified over
280 834 cysteine-containing peptides (Figure 3B and source data 1). Of these
281 peptides, 771 exhibited pair-labeling with an overall average H/L ratio 2.6, and
282 348 peptides (45%) displayed high ratios (H/L>2). These findings confirmed that
283 ATF4 drives global changes in protein sulfhydration in MIN6 cells.

284 Sulfhydrated cysteine residues in proteins may contribute to their biological
285 activities, especially when these modified cysteine residues reside within
286 functional domains. We thus queried the Uniprot database to retrieve functional
287 annotations for the aforementioned 827 peptides. The analysis revealed that 28%
288 of the peptides were localized to protein regions whose structural and functional
289 properties are known (Figure 3C, Figure 3-figure supplement 1). An additional
290 18% were found within functional regions of proteins with cysteine residues of
291 unknown significance. Our finding of sulfhydration of specific cysteine residues
292 within functional domains of proteins suggests that the cysteine modification
293 influences the activity of proteins. In contrast, 4.2% of the peptides in question
294 contained cysteine residues in experimentally proven active sites of enzymes or
295 cysteine residues involved in disulfide bond formation (Figure 3C). This
296 percentage of active cysteine-containing peptides from the BTA assay is
297 significantly larger than the 0.2% of all cysteines in the Uniprot database that
298 have been assigned to experimentally characterized active cysteines
299 (Weerapana et al., 2010). Finally, 2.4% of the annotated peptides were found in
300 known nucleotide binding domains of proteins, suggesting the potential for

301 regulation of gene expression by H₂S cysteine-modified proteins. None of these
302 proteins have been reported as targets of sulfhydration. Although not found
303 among the 827 peptides in this study, the NF- κ B RelA transcription factor has
304 been shown to be sulfhydrated in the DNA-binding domain, resulting in increased
305 DNA-binding activity (Sen et al., 2012). We also found by querying the redox
306 modification databases (RedoxDB and GPS-SNO) that 11% of the 834 peptides
307 from the RedoxDB and 36% from the GPS-SNO corresponded to cysteine
308 residues that are known to be modified by nitrosylation or glutathionylation
309 (Figure 3B, Figure 3-figure supplement 2). Taken together, these data indicate
310 that protein sulfhydration not only influences the catalytic activity of enzymes like
311 GAPDH, but potentially can regulate a broad range of biological processes.

312 We noted a wide range of H/L ratios in the identified peptides, reflecting a large
313 difference in the reactivity of individual cysteines to sulfhydration in MIN6 cells
314 that overexpress ATF4 (Figure 3B-D). In addition, labeled cysteines on the same
315 protein exhibited remarkably different ratios (Figure 3-figure supplement 3). For
316 example, the protein, PHGDH, was labeled on two cysteines, Cys²⁸¹ had an H/L
317 ratio of 5.8, whereas Cys²⁵⁴ displayed a ratio of 17. To identify a sulfhydration
318 motif in proteins, all cysteine-containing peptides (Figure 3B) were analysed by
319 the pLogo motif analyzer program. This analysis did not reveal conserved
320 residues surrounding the modified cysteine site (Figure 3-figure supplement 4A),
321 a result consistent with other enzyme-independent oxidative modifications of
322 cysteines (Weerapana et al., 2010) (Marino and Gladyshev, 2011). However,
323 when we selected only the peptides with high H/L ratios (>2), and searched for a

324 sequence motif at the cysteine modification sites (Figure 3-figure supplement 4B),
325 an Arg residue was significantly enriched at the +1 position of the modified
326 cysteine (Figure 3-figure supplement 4B). Additionally, structure motif and
327 surface accessibility analysis revealed that the modified cysteine is highly
328 accessible and positioned at the N-terminal alpha-helices (Figure 3-figure
329 supplement 4C-D). This is consistent with previous reports suggesting that a
330 reactive cysteine thiolate anion is stabilized by interaction with alpha-helix dipoles
331 (Kortemme and Creighton, 1995; Weerapana et al., 2010).

332 Bioinformatics clustering with two pathway annotation programs DAVID and
333 Ingenuity Pathway Analysis (IPA) revealed an enrichment of sulfhydrated
334 proteins in glycolysis and mitochondrial oxidative metabolism (Figure 3E, Figure
335 3-figure supplement 5). Data from this analysis are in agreement with increased
336 activity of the glycolytic enzyme, GAPDH, by sulfhydration, and prompted the
337 question as to whether or not glycolytic flux is regulated by the H₂S-dependent
338 modification of enzymes involved in intermediary metabolism. Also in agreement
339 with this hypothesis, we found that ATF4-overexpressing MIN6 cells had higher
340 glycolytic rates as evaluated with a Seahorse analyzer (Figure 4-figure
341 supplement 1). Furthermore, the activity of the rate-limiting glycolytic enzyme,
342 pyruvate kinase 2 (PKM2), also was increased in ATF4 overexpressing MIN6
343 cells, in a manner dependent on CTH activity (Figure 4-figure supplement 2). We
344 therefore returned to the induction of ER stress by Tg-treatment of MIN6 cells
345 and evaluated glycolytic flux rates in the absence or presence of PAG. The
346 advantage of using PAG instead of genetic manipulation such as gene

347 knockdown is that the inhibitor could be added at the same time as labeled
348 glucose, thus allowing assessment of the inhibitor's effect on glycolytic flux rates.
349 We directly measured changes in metabolic flux by utilizing stable isotope label
350 incorporation and mass isotopomer analyses. MIN6 cells were treated with Tg for
351 18 h; the growth media was changed to (D-glucose-¹³C₆) media in the presence
352 or absence of PAG during the last 3.5 h of treatment. Tg-treatment significantly
353 augmented glycolytic flux as determined by the increase in the glycolytic
354 intermediate, 3 phosphoglyceric acid (3PG), as well as lactate and alanine
355 (Figure 4A-C, Supplementary File 1). The flux was consistent with an increase in
356 the relative concentrations of 3PG and alanine (Figure 4B, Supplementary File
357 1). However, lactate levels were decreased significantly despite the increased
358 flux. A decrease in cellular lactate levels supports the idea that there is high
359 consumption of pyruvate by the mitochondria to generate oxaloacetate (OAA). In
360 contrast to the increased glycolytic rates, flux to Tricarboxylic Acid Cycle (TCA)
361 intermediates was significantly reduced by Tg-treatment as evidenced by the low
362 ¹³C label incorporation of both acetyl-CoA and OAA moieties of citrate, fumarate,
363 and malate (Figure 4A-B, Supplementary File 1). When the cells were exposed to
364 PAG along with Tg-treatment, the increase in glycolytic flux was prevented, as
365 shown by the decrease in ¹³C-labeling of 3PG, lactate, and alanine. In contrast,
366 TCA cycle flux was restored, as exemplified by the increase in ¹³C-labeling of
367 both OAA and acetyl-CoA moieties of citrate, succinate, fumarate, and malate,
368 and a decrease in their concentrations, suggesting utilization. ¹³C-labeling of
369 aspartate and glutamine also increased significantly, indicating increased

370 cataplerosis of TCA cycle intermediates. Moreover, we determined the activity of
371 PKM2 in MIN6 cells treated with Tg in the presence or absence of PAG. Tg-
372 treatment increased PKM2 activity, but PAG addition inhibited the increase,
373 without affecting PKM2 protein levels (Figure 4-figure supplement 3). These data
374 suggest that ER stress, via H₂S-mediated signaling, promotes glycolysis and
375 decreases mitochondrial oxidative metabolism.

376

377 **Discussion**

378 In summary, sulfhydration of specific cysteines in proteins is a key function of
379 H₂S (Kabil and Banerjee, 2010; Paul and Snyder, 2012; Szabo et al., 2013).
380 Thus, the development of tools that can quantitatively measure genome-wide
381 protein sulfhydration in physiological or pathological conditions is of central
382 importance. However, a significant challenge in studies of the biological
383 significance of protein sulfhydration is the lack of an approach to
384 selectively detect sulfhydrated cysteines from other modifications (disulfide
385 bonds, glutathionylated thiols and sulfenic acids) in complex biological samples.
386 In this study, we introduced the BTA approach that allowed the quantitative
387 assessment of changes in the sulfhydration of specific cysteines in the proteome
388 and in individual proteins. BTA is superior to other reported methodologies that
389 aimed to profile cysteine modifications, such as the most commonly used, a
390 modified biotin switch technique (BST). BST was originally designed to study
391 protein nitrosylation and postulated to differentiate free thiols and persulfides
392 (Mustafa et al., 2009). A key advantage of BTA over the existing methodologies,

393 is that the experimental approach has steps to avoid false-positive and negative
394 results, as target proteins for sulfhydration. BST is commonly generating such
395 false targets for cysteine modifications (Forrester et al., 2009; Sen et al., 2012).
396 Using multiple validations, our data support the specificity and reliability of the
397 BTA assay for analysis of protein sulfhydration both in vitro and in vivo. With this
398 approach, we found that ATF4 is the master regulator of protein sulfhydration in
399 pancreatic β cells during ER stress, by means of its function as a transcription
400 factor. A large number of protein targets have been discovered to undergo
401 sulfhydration in β cells by the BTA approach. Almost 1,000 sulfhydrated cysteine-
402 containing peptides were present in the cells under the chronic ER stress
403 condition of treatment with Tg for 18 h. Combined with the isotopic-labeling
404 strategy, almost 820 peptides on more than 500 proteins were quantified in the
405 cells overexpressing ATF4. These data show the potential of the BTA method for
406 further systematic studies of biological events. To our knowledge, the current
407 dataset encompasses most known sulfhydrated cysteine residues in proteins in
408 any organism. Our bioinformatics analyses revealed sulfhydrated cysteine
409 residues located on a variety of structure-function domains, suggesting the
410 possibility of regulatory mechanism(s) mediated by protein sulfhydration.
411 Structure and sequence analysis revealed consensus motifs that favor
412 sulfhydration; an arginine residue and alpha-helix dipoles are both contributing to
413 stabilize sulfhydrated cysteine thiolates in the local environment.
414 Pathway analyses showed that H₂S-mediated sulfhydration of cysteine residues
415 is that part of the ISR with the highest enrichment in proteins involved in energy

416 metabolism. The metabolic flux revealed that H₂S promotes aerobic glycolysis
417 associated with decreased oxidative phosphorylation in mitochondria during ER
418 stress in β cells. The TCA cycle revolves by the action of the respiratory chain
419 that requires oxygen to operate. In response to ER stress, mitochondrial function
420 and cellular respiration are down-regulated to limit oxygen demand and to
421 sustain mitochondria. When ATP production from the TCA cycle becomes limited
422 and glycolytic flux increases, there is a risk of accumulation of lactate from
423 pyruvate. One way to escape accumulation of lactate is the mitochondrial
424 conversion of pyruvate to oxalacetic acid (OAA) by pyruvate carboxylase. This
425 latter enzyme was found to be sulfhydrated, consistent with the notion that
426 sulfhydration is linked to metabolic reprogramming towards glycolysis.

427 The switch of energy production from mitochondria to glycolysis is known as a
428 signature of hypoxic conditions. This metabolic switch has also been observed in
429 many cancer cells characterized as the Warburg effect, which contributes to
430 tumor growth. The Warburg effect provides advantages to cancer cell survival via
431 the rapid ATP production through glycolysis, as well as the increased conversion
432 of glucose into anabolic biomolecules (amino acid, nucleic acid and lipid
433 biosynthesis) and reducing power (NADPH) for regeneration of antioxidants.,
434 This metabolic response of tumor cells contributes to tumor growth and
435 metastasis (Vander Heiden et al., 2009). By analogy, the aerobic glycolysis
436 triggered by increased H₂S production could give β cells the capability to acquire
437 ATP and nutrients to adapt their cellular metabolism towards maintaining ATP
438 levels in the ER (Vishnu et al., 2014), increasing synthesis of

439 glycerolphospholipids, glycoproteins and protein (Krokowski et al., 2013b), all
440 important components of the ISR. Similar to hypoxic conditions, a phenotype
441 associated with most tumors, the decreased mitochondria function in β cells
442 during ER stress, can also be viewed as an adaptive response by limiting
443 mitochondria ROS and mitochondria-mediated apoptosis. We therefore view that
444 the H₂S-mediated increase in glycolysis is an adaptive mechanism for survival of
445 β cells to chronic ER stress, along with the improved ER function and insulin
446 production and folding, both critical factors controlling hyperglycemia in diabetes.
447 Future work should determine which are the key proteins targeted by H₂S and
448 thus contributing to metabolic reprogramming of β cells, and if and how insulin
449 synthesis and secretion is affected by sulfhydrylation of these proteins during ER
450 stress.

451 Abnormal H₂S metabolism has been reported to occur in various diseases,
452 mostly through the deregulation of gene expression encoding for H₂S-generating
453 enzymes (Wallace and Wang, 2015). An increase of their levels by stimulants is
454 expected to have similar effects on sulfhydrylation of proteins like the ATF4-
455 induced CTH under conditions of ER stress. It is the levels of H₂S under
456 oxidative conditions that influence cellular functions. In the present study, ER
457 stress in β cells induced elevated Cth levels, whereas CBS was unaffected. The
458 deregulated oxidative modification at cysteine residues by H₂S may be a major
459 contributing factor to disease development. In this case, it would provide a
460 rationale for the design of therapeutic agents that would modulate the activity of
461 the involved enzymes.

462

463

464 **Materials and Methods**

465 **Mouse Islets RNA isolation**

466 Experimental protocols were approved by the Case Western Reserve University
467 Institutional Animal Care and Use Committee. C57BL/6J and C57BL/6-*Ins2*^{+/*Akita*}
468 mice were used for experiments. Mice from the Jackson Laboratory were bred at
469 the animal facilities at Case Western Reserve University and were fed standard
470 lab chow (LabDiet). Mice were housed under 12:12 h light/dark cycle with free
471 access to food and water at 23°C. Mouse pancreatic islets were isolated as
472 described before (Krokowski et al., 2013a). Islets from 6 weeks old male
473 C57BL/6-*Ins2*^{+/*Akita*} (n=6) and age and sex matched wild type (n=6) were cultured
474 for 2 h in RPMI 1640 media supplemented with 10% FBS and 5 mM glucose
475 before RNA isolation. For Tg treatment (1 µM), islets from wild type mice (n=6)
476 were combined and cultured in RPMI 1640 medium supplemented with 10% FBS
477 in atmosphere of 5% CO₂ at 37°C for 24 h. From each group 150-200 islets were
478 manually picked and used for RNA isolation. Islets were treated with
479 QIAshredder (Qiagen), and RNA was purified using the RNeasy Plus Micro kit
480 (Qiagen).

481

482 **Human Islets RNA isolation**

483 Institutional review board approval for research use of isolated human islets was
484 obtained from the University of Michigan. Human islets were isolated from
485 previously healthy, nondiabetic organ donors by the University of Chicago
486 Transplant Center. The islets were divided into two groups, incubated in CMRL

487 medium containing either 5.5 mM glucose with or without Tg (1 μ M), for 24 h.
488 The islets were frozen at -80°C before analysis. RNA was isolated as described
489 above from 200 islets/treatment.

490

491 **RT-qPCR analysis of mRNAs for MIN6 cells**

492 RNA was isolated from mouse MIN6 cells using TRIzol (Invitrogen). cDNA was
493 synthesized from total RNA isolated from islets or MIN6 cells using the
494 SuperScript III First-Strand Synthesis Super Mix (Invitrogen), and the abundance
495 of cDNA isolated from each sample was quantified by qPCR using the VeriQuest
496 SYBR Green qPCR Master Mix (Affymetrix) with the StepOnePlus Real-Time
497 PCR System (Applied Biosystems).

498

499 **Cell Culture and viral particles**

500 MIN6 cells were cultured in high glucose DMEM supplemented with 10% FBS, 2
501 mM L-glutamine, 1 mM sodium pyruvate, 55 μ M β -mercaptoethanol, 100 units/ml
502 penicillin, and 100 μ g/ml streptomycin at 37°C in atmosphere of 5% CO₂. β -
503 mercaptoethanol was removed from the media 12 h before experimentation. Rat
504 INS1 cells were cultured in RPMI 1640 supplemented with 11 mM glucose, 10%
505 heat inactive FBS, 2 mM L-glutamine, 1 mM sodium pyruvate, 100 units/ml
506 penicillin, and 100 μ g/ml streptomycin at 37°C in atmosphere of 5% CO₂. Tg
507 (Sigma-Aldrich) was used at 400 nM and the Cth inhibitor - DL-propargylglycine
508 (PAG, Sigma Aldrich) at 3 mM. Lentiviral particles were prepared in HEK293T as
509 described before (Saikia et al., 2014). Lentiviral vector expressing shRNA against

510 *ATF4* were obtained from Sigma-Aldrich (TRCN0000301646). Adenovirus
511 mediated shRNA against mouse CTH (shRNA sequence:
512 CCGGCCATTACGATTACCCATCTTTCTCGAGAAAGATGGGTAATCGTAATGG
513 TTTTTG) was purchased from Vector Biolabs. MIN6 cells were infected in the
514 presence of 10 µg/ml polybrene and selection with 2.5 µg/ml puromycin (Life
515 Technologies) was conducted 24 h post-infection for 5 days. Adenovirus particles
516 for expression of β galactosidase (β-Gal), GFP or mouse ATF4 protein were
517 prepared in HEK293 cells and were used for infection as described before (Guan
518 et al., 2014).

519

520 **Bacterial expression of wild type and Cys¹⁵⁰Ser human recombinant**

521 **GAPDH**

522 Human GST-tagged wild type or C¹⁵⁰S GAPDH mutant (Hara et al., 2005) were
523 expressed in the *E. coli* BL21 strain. Protein expression was induced by addition
524 of IPTG (100 µM). When bacterial cultures reached OD₆₀₀ of 0.8 at 37 °C, IPTG
525 was added for 4 h incubation before lysis in a buffer containing 50 mM Tris-HCl
526 (pH 7.5) and 1 mM EDTA. Lysates were centrifuged and applied on a buffer-
527 equilibrated GST-sepharose affinity spin column (Pierce). After extensive washes
528 to remove unbound protein, recombinant GAPDH was released by digestion with
529 thrombin protease (Sigma). The protein purity was determined on SDS/PAGE
530 gels stained by Coomassie blue.

531

532 **GAPDH activity assay**

533 The specific activity of GAPDH was determined as described before (Hara et al.,
534 2005). Recombinant protein (50 nM) was used for the in vitro activity assays. To
535 test the GAPDH activity in cell lysates, MIN6 cells were harvested in RIPA buffer
536 (150 mM NaCl, 1 mM EDTA, 1 % Triton X-100, 0.5 % deoxycholic acid, 50 mM
537 Tris-HCl, pH 7.5), sonicated on ice and centrifuged at 4°C. 1-20 µg of protein
538 lysate was used for the activity assays. The reaction mixture contained 100 mM
539 Tris-HCl (pH 7.5), 5 mM MgCl₂, 3 mM 3-phosphoglycerate, 5 units/ml of *S.*
540 *cerevisiae* 3-phosphoglycerate kinase (PGK, Sigma-Aldrich), 2 mM ATP and
541 0.25 mM NADH. Reactions were conducted in 200 µl volume at 25°C and
542 monitored spectrophotometrically at 340 nm for 3 min using a M3 microplate
543 reader (Molecular Devices).

544

545 **PKM activity assay**

546 PKM activity was tested in the cell extracts as described (Anastasiou et al.,
547 2011). MIN6 cells were collected by trypsinization and the cell pellets were
548 washed twice with cold PBS. Cells were resuspended in RIPA buffer, sonicated
549 on ice and subjected to a quick centrifugation at 4°C. Reaction mixtures
550 contained 50 mM Tris-HCl (pH 7.5), 100 mM KCl, 5 mM MgCl₂, 0.5 mM ADP, 0.2
551 mM NADH, 8 units of lactate dehydrogenase (Sigma-Aldrich), and 1-10 µg of cell
552 lysate. The enzymatic reaction was initiated by the addition of PEP
553 (phosphoenolpyruvic acid, 0.5 mM) as the substrate. The oxidation of NADH was
554 monitored at 340 nm for 3 min using a M3 microplate reader (Molecular Devices).

555

556 **Activity of cystine/glutamate exchanger Slc7a11**

557 The activity of the amino acid transporter was tested as described before
558 (Krokowski et al., 2013a). Uptake of Glu was tested in the absence of Na⁺ ions
559 (EBSS solution, NaCl replaced with choline chloride), with 100 μM Glu and 4
560 μCi/ml of ³H-Glu (Parkin Elmer) for 3 min at 37°C. MIN6 cells were washed twice
561 with cold PBS then amino acids were extracted with ethanol and radioactivity
562 was counted. The specific activity was normalized to protein content that was
563 determined by the Lowery assay.

564

565 **Intracellular glutathione content and the ratio of oxidized and reduced**
566 **glutathione**

567 MIN6 cells (6x10⁴ cell per well) were seeded into 96-well plates. After 48 h the
568 growth media was removed, the total glutathione contents and GSH/GSSG ratios
569 were determined with the GSH/GSSG-Glo Tm assay from Promega.

570

571 **ROS Measurements**

572 Total intracellular levels of ROS were quantified using dichlorofluorescein
573 diacetate (CM-H₂DCFDA; 10 μM). MIN6 cells were seeded into 96-well plates.
574 After 48 h, cells were washed with warm PBS and incubated with the dye in
575 phenol-red free DMEM without FBS. After 1 h, the cells were washed with PBS to
576 remove the dye and placed in phenol-red free DMEM. CM-H₂DCFDA
577 fluorescence was measured at excitation/emission wavelengths of 495/517 nm.
578 Cells not exposed to the probe were used to test the background fluorescence.

579 After subtraction of background fluorescence results were normalized to protein
580 content determined by the BCA assay.

581

582 **H₂S-production assays**

583 Frozen cell pellets were lysed in 100 mM HEPES (pH 7.4), to obtain a lysate
584 concentration of 100 mg/ml. H₂S production was measured as described
585 previously (Kabil et al., 2011). Briefly, reactions containing cell lysate (200 µl), 10
586 mM cysteine and 100 mM HEPES (pH 7.4) were prepared in 20-ml
587 polypropylene syringes in a total reaction volume of 400 µl. Reactions were
588 started with the addition of cysteine. Syringes were sealed and the headspace
589 was flushed with nitrogen 5 times by using a three-way stopcock, and left in
590 nitrogen in a final total volume (aqueous + gas) of 20 ml. Syringes were placed at
591 37°C in a shaker incubator (75 rpm) for 20 min. Control reactions without cell
592 lysates were prepared in parallel. Aliquots of 0.2 ml from the gas phase were
593 collected through a septum attached to the stopcock, and injected in an HP 6890
594 gas chromatograph (GC) (Hewlett Packard) equipped with a DB-1 column
595 (30 m×0.53 mm×1.0 µm). Flow rate of the carrier gas (helium) was 1 ml/min, and
596 the temperature gradient ranged from 30°C to 110°C over a 20-min period. H₂S
597 was detected by a 355 sulfur chemiluminescence detector (Agilent) attached to
598 the GC. H₂S standard gas (Cryogenic Gases, Detroit, MI) with a stock
599 concentration of 40 ppm (1.785 µM) in nitrogen was used to generate a standard
600 curve. The amount of H₂S in the injected volume was calculated from the peak
601 areas by using the calibration coefficient obtained from the standard curve.

602 Ionized H₂S concentration in the liquid phase was calculated for the pH of the
603 reaction mixture (pH 7.4) by using a pK_a value of 6.8 for ionization of H₂S. The
604 resulting H₂S concentration in the total reaction volume was then used to obtain
605 the specific activity expressed as nmol H₂S per mg protein per min.

606

607 **Biotin Thiol Assay**

608 In order to detect and identify sulfhydrated proteins from MIN6 cells, cells were
609 lysed with the RIPA buffer (150 mM NaCl, 1 mM EDTA, 0.5 % Triton X-100, 0.5
610 % deoxycholic acid and 100 mM Tris-HCl (pH 7.5) containing protease and
611 phosphatase inhibitor from Roche. Cells were sonicated on ice, lysates were
612 clarified by centrifugation at 4°C and the protein concentrations were determined
613 by the BCA assay (BioRad). Equal amount (4 mg) of proteins was incubated
614 with 100 µM NM-biotin (Pierce) for 30 min with occasionally gentle mixing at
615 room temperature and subsequently precipitated by cold acetone. After
616 centrifugation, pellets of precipitated proteins were washed with 70% cold
617 acetone twice, and then suspended in buffer (0.1% SDS, 150 mM NaCl, 1 mM
618 EDTA and 0.5% Triton X-100, 50 mM Tris-HCl, pH 7.5) mixed with Streptavidin-
619 agarose resin (Thermo Scientific) and kept rotating overnight at 4°C. The beads
620 were washed 5 times with wash buffer 1 (0.5 % Triton x-100, 150 mM NaCl, 50
621 mM Tris-HCl, pH 7.5) followed by 5 washes with wash buffer 2 (0.5% Triton X-
622 100, 600 mM NaCl, 50 mM Tris-HCl, pH 7.5). Resin with bound proteins was
623 incubated with 500 µl of the elution buffer with or without 20 mM DTT for 30 min
624 at 25°C. Eluted proteins were concentrated to a final volume of 25-40 µl with

625 utilization of Amicon Ultracel 10K (Millipore) and used for gel electrophoresis
626 followed by either western blot or MS analysis.

627

628 **Red maleimide assay**

629 The assay was previously described (Sen et al., 2012) and modified in order to
630 adapt to our experimental needs. Purified recombinant GAPDH was next treated
631 with either 50 μ M NaCl as control, 50 μ M NaHS or 50 μ M H₂O₂ for 45 min at
632 room temperature. After desalting through a spin column (Pierce), the samples
633 were incubated with 1 μ M red maleimide probe (Alexa Fluor 680 C₂ Maleimide,
634 Molecular Probes) for 20 min at room temperature. After the incubation, these
635 samples were treated with or without 10 mM β -mercaptoethanol and the reaction
636 was stopped by the addition of 100 mM iodoacetamide. Samples were
637 suspended in sample buffer for non-reducing gel electrophoresis. After
638 electrophoretic separation, the gel was scanned with the Li-COR Odyssey
639 system. The intensity of red fluorescence of GAPDH was quantified with the
640 Odyssey system software. Subsequently proteins from the gel were transferred
641 on a PVDF membrane and subjected to Western blot analysis for GAPDH.

642

643 **Purification of H₂S-modified cysteine-containing peptides from MIN6 cells**

644 In order to identify H₂S-modified cysteine-containing peptides from cell lysates,
645 proteins were extracted and biotinylated as described above. Biotinylated
646 proteins were precipitated with ice cold acetone, resuspended in denaturation
647 buffer (30 mM Tris-HCl (pH 7.5), 8 M urea and 1 mM MgSO₄) as described

648 (Morisse et al., 2014), diluted with 10 volumes of the buffer (30 mM Tris-HCl (pH
649 7.5), 1 mM EDTA and 200 mM NaCl) and incubated with modified porcine trypsin
650 (Promega) with occasionally mixing for 18 h at 30°C. The ratio of the enzyme to
651 substrate was 1:80 (w/w). After digestion, trypsin was inactivated by incubation at
652 95°C for 10 min then reactions were mixed with the streptavidin-agarose beads
653 (500 µl) and incubated at 4°C for 18 h following extensive washes in the
654 presence of 0.1% SDS as described above. Peptides were eluted with 20 mM
655 ammonium bicarbonate supplemented with 10 mM DTT after 25 min incubation
656 at room temperature. DTT was removed with utilization of a C-18 column
657 (Pierce). Peptides were eluted from the desalting column with acetonitrile, dried
658 under vacuum and suspended in buffer (30 mM Tris-HCl (pH 7.5), 1mM EDTA
659 and 150 mM NaCl). Free -SH groups were alkylated by NEM (either deuterium or
660 hydrogen containing) at final concentrations of 40 mM. The alkylated peptides
661 were concentrated with a C-18 column (Pierce) for LC-MS/MS analysis.

662

663 **Liquid-chromatography-mass-spectrometry (LC-MS/MS) analysis**

664 LC-MS/MS analysis was performed on an LTQ-Orbitrap Elite mass spectrometer
665 (Thermo-Fisher) coupled to an Ultimate 3000 high-performance liquid
666 chromatography system. Protein digests were loaded onto a 75 µm desalting
667 column packed with 2 cm of Acclaim PepMap C18 reverse phase resin (Dionex).
668 The peptides were then eluted onto a Dionex 15 cm x 75 µm id Acclaim Pepmap
669 C18, 2µm, 100 Å reversed- phase capillary chromatography column using a
670 gradient of 2–80% buffer B in buffer A (buffer A: 0.1% formic acid; buffer B: 5%

671 water, 95% acetonitrile, 0.1% formic acid). The peptides were then eluted from
672 the C18 column into the mass spectrometer at a flow rate of 300 nl/ min and the
673 spray voltage was set to 1.9 kV. One full MS scan (FTMS) (300–2,000 MW) was
674 followed by 20 data dependent scans (ITMS) of the *n*th most intense ions with
675 dynamic exclusion enabled.

676

677 **Peptide identification**

678 Peak lists were extracted from Xcaliber RAW files using Proteome Discoverer
679 1.4. These peak lists were searched Sequest HT and Mascot (2.3) search
680 engines. The data was searched against the mouse reference sequence
681 database which contains 77807 entries using a precursor ion tolerance of 10
682 ppm and a fragment ion tolerance of 0.6 Da. These searches included
683 differential modification of +125.047679 and +130.079062 on cysteine to account
684 for NEM and d₅-NEM alkylation and +15.994915 Da to account for oxidation on
685 methionine residues. Peptide identification was validated with the Percolator
686 node on the basis of q-values which are estimated from target-decoy
687 searches. The false discovery rate (FDR) for these searches was set to 1% at
688 the peptide level. In addition, peptides were also required to be fully tryptic and
689 have Xcorr scores > 1.5 (+1), 2.0 (+2), 2.25 (+3), and 2.5 (+4).

690

691 **Ratio quantification**

692 Quantification of light/heavy ratios (d₅-NEM/NEM) was performed using two
693 algorithms of Proteome Discoverer, the event detector and Precursor Ions

694 Quantifier. The event detector applied a 2 ppm mass variability and 0.2 minute
695 chromatographic window for the generation of extracted ion
696 chromatograms. The Peptide ratio was calculated from the summed extracted
697 ion chromatograms of all isotopes for the NEM and d₅-NEM containing
698 peptides. All missing ions were assigned a value equivalent to the minimum
699 intensity, only unique peptides were quantified, and since this included
700 quantitation at the peptide level, single channel was used. The H/L ratios of
701 approximately 25% of the quantified peptides were manually validated.

702

703 **Bioinformatics analysis of cysteine-containing peptides**

704 For functional annotation: Protein sequences from the FTP site of the Uniprot
705 Protein database for mouse (Proteome_ID/Tax_ID: UP000000589/10090), rat
706 (Proteome_ID/Tax_ID: UP000002494/10116) and human (Proteome_ID/Tax_ID:
707 UP000005640/9606) release current as of May 23 2015. Sequence annotation
708 in the feature fields (ACT_SITE, BINDING, CA_BIND, DISULFID, DNA_BIND,
709 DOMAIN, METAL, MOD_RES, MOTIF, NP_BIND, SITE, ZN_FING) of the
710 Uniprot entry was searched and any annotation corresponding to the labeled
711 cysteine peptides was collected.

712 For redox cysteine annotation: each peptide identified by MS, all exact matches
713 in any of the RedoxDB databases on any oxidative modification cysteine
714 sequences (fasta or additional_fasta) were collected. For motif search: The larger
715 data set of putative modification cysteine sites and their vicinity sequences were

716 submitted to the pLogo program (www.plogo.uconn.edu, version v1.2.0) (O'Shea
717 et al., 2013) to identify linear motif.

718 For prediction of candidate peptides for nitrosylation: the peptide sequences with
719 H/L ratio >2 were submitted for use in predicting nitrosylation sites under the
720 medium threshold condition using the batch prediction tool of the GPS-SNO 1.0
721 software (Xue et al., 2010). The predicted nitrosylation sites of sequences were
722 extracted for further analysis.

723 For determination of surface accessibility and secondary structural motif: we
724 turned to DSSP's (Kabsch and Sander, 1983; Touw et al., 2015) annotations of
725 the PDB (Berman et al., 2000). We downloaded a total of 108355 DSSP-
726 annotated PDB files from (rsync.cmbi.ru.nl/dssp/) on Sep. 9th 2015. Each
727 peptide with H/L greater than 2-fold was aligned on all matching DSSP profiles,
728 from which the 10-state structural context and accessibility were extracted. When
729 an exact match is not found, then all matches with 1 mismatch are considered.
730 The structural context of a peptide is defined as the context that reoccur most
731 frequently among the hits, while the accessibility is the average across the hits,
732 \log_2 -normalized by the median of accessibility considering the amino acid type;
733 positive \log_2 values means that the amino acid embedded in the 3D structure of
734 the protein is more accessible than the mode (median).

735 For pathway annotation: the canonical pathways were scored based on the total
736 sulfhydrated peptides and the peptides with H/L ratios greater than 2 by using
737 DAVID (www.david.ncifcrf.gov) and Ingenuity Pathway Analysis (IPA,
738 www.qiagen.com/ingenuity) programs. Statistical significant of pathways are

739 calculated and pathways are ranked by the p -values based on those tests. The
740 tests measure the likelihood that the association between proteins measured in
741 our experiments and a pathway is due to random chance. The smaller the p -
742 value the less likely that the association is due to random chance. Top scoring
743 pathways are presented.

744

745 **Metabolic labeling of MIN6 cells**

746 MIN6 cells were plated onto 10-cm plates in triplicates and cultured in the cell
747 growth medium. After 48 h treatment with Tg, metabolic labeling was performed.
748 Cells were washed with warm PBS and incubated for 3 h in the DMEM medium
749 containing 10% heat inactive FBS, 2 mM glutamine, and 25 mM glucose
750 consisting of a mixture of 12.5 mM D-glucose plus 12.5 mM of D-[U-¹³C] glucose.
751 After incubation, cells were washed with PBS, followed by trypsinization. Cells
752 were pelleted by centrifuging at 4°C for 5 min at 650 x g , and pellets were stored
753 at -80°C until extraction of metabolites.

754

755 **Assay of media [U-¹³C] glucose enrichment**

756 Glucose isotopic enrichment was determined following (van Dijk et al., 2001) with
757 modifications. Briefly, glucose was extracted by the addition of 500 μ l of ice-cold
758 ethanol to 50 μ l of media. Samples were mixed and incubated on ice for 30 min.
759 Samples were centrifuged at 4°C for 10 min at 14,000 rpm and ethanol was
760 transferred to a GC/MS vial and evaporated to dryness in a SpeedVac
761 evaporator. Glucose was converted to its pentaacetate derivative by the reaction

762 with 150 μ l of acetic anhydride in pyridine (2:1, v/v) at 60°C for 30 min. Samples
763 were evaporated to dryness and glucose derivatives were reconstituted in 80 μ l
764 of ethyl acetate and transferred to GC/MS inserts. Samples were injected in
765 duplicate and masses 331-337, containing M0...M+5 isotopomers were
766 monitored. Enrichment was determined as a ratio of (M+5) / (Σ_{M0-M5}).

767

768 **Metabolite extraction**

769 Metabolites were extracted following (Yang et al., 2008) with modifications.
770 Briefly, cellular pellets in Eppendorf tubes were homogenized and frozen in 600
771 μ l of Folch solution (chloroform:methanol, 2:1, vol./vol.) on dry ice. After addition
772 of 0.4 volumes of ice-cold water, cells were homogenized again and let sit on ice
773 for 30 min. Homogenates were centrifuged at 4°C for 10 min at 14,000 rpm. The
774 upper methanol/water layer was removed to GC/MS vial. To the bottom
775 chloroform layer, 120 μ l of water and 200 μ l of methanol were added and
776 extraction steps from above were repeated. Combined methanol/water layers
777 were evaporated to dryness in Speedvac evaporator at 4°C. Metabolites were
778 derivatized using two-step derivatization. First, keto- and aldehyde groups were
779 protected by the reaction with MOX (methoxylamine-HCl in pyridine, 1:2)
780 overnight at room temperature. Then excess derivatizing agent was evaporated
781 and dry residue was converted to MOX-TMS (trimethylsilyl) derivative by reacting
782 with bis(trimethylsilyl) trifluoroacetamide with 10% trimethylchlorosilane (Regisil)
783 at 60°C for 20 min. Resulting MOX-TMS derivatives were run in GC-MS.

784

785 **GC-MS conditions**

786 Analyses were carried out on an Agilent 5973 mass spectrometer equipped with
787 6890 Gas Chromatograph. A DB17-MS capillary column (30 m × 0.25 mm × 0.25
788 μm) was used in all assays with a helium flow of 1 ml/min. Samples were
789 analyzed in Selected Ion Monitoring (SIM) mode using electron impact ionization
790 (EI). Ion dwell time was set to 10 msec. The following metabolites were
791 monitored: Glycerol 3 phosphate (G3P), 3 Phosphoglycerate (3PG), Lactate,
792 Alanine, Citrate, Succinate, Fumarate, Malate, Glycine, and Serine.

793

794 **Mitochondrial oxidative phosphorylation and glycolysis**

795 MIN6 cells were diluted to 80 000 cells/well in a Seahorse tissue culture system
796 in the presence of either *GFP* or *ATF4* overexpression. Cells were plated 2 days
797 prior to experimentation. The cells were washed with warm PBS and then
798 incubated for 30 min at 37°C and ambient CO₂ in HCO₃-free DMEM containing
799 25 mM glucose, 2 mM glutamine, 1 mM pyruvate (pH 7.4). Cells were then
800 treated sequentially with oligomycin (0.2 μg/ml), carbonyl cyanide 4-
801 (trifluoromethoxy) phenylhydrazone (FCCP, 1 μM) and rotenone (1 μM). The
802 rates of mitochondrial respiration and cellular acidification were determined by
803 using the Seahorse extracellular flux analyzer (Seahorse Bioscience, North
804 Billerica, MA). Corrected oxygen consumption rate (OCR) and extracellular
805 acidification rate (ECAR) values were normalized to cell number.

806

807 **Other methods**

808 MIN6 cells extracts for protein immunodetection were obtained after cell lysis in
809 RIPA buffer as described before (Krokowski et al., 2013a). Protein content was
810 determined by the BCA assay (BioRad). Mouse islet protein extracts were
811 extracted in RIPA buffer. From approximately 100 islets the same amount of
812 extracts determined by measuring DNA content with the Quant-iT dsDNA assay
813 kit (Molecular Probes) and equal DNA amount was used for immunodetection.
814 Western blotting was performed as described before (Krokowski et al., 2013a).
815 Anti-Actin (ab 3280) antibodies were from Abcam. Anti-Cth (H00001491) and
816 anti-CBS (H00000875) were from Abnova. Antibodies against: PERK (3192),
817 phospho PERK (3179) and PKM2 (4053) were purchased from Cell Signaling.
818 Anti-ATF4 (sc-200), anti-GAPDH (sc-32233), anti-eIF2 α (sc-133227) and XBP1
819 (sc-7160) were from Santa Cruz Biotechnology. Antibodies against
820 phosphorylated eIF2 α (NB 110-56949) and Ero1 α (NB 100-2525) were obtained
821 from Novus and anti-tubulin (T9026) serum was from Sigma-Aldrich.

822

823 **Acknowledgments**

824 We thank Dr. Jonathan S. Stamler for providing valuable comments in the
825 development of methodology. Dr. John J. Mieyal provided suggestions for
826 GAPDH glutathionylation study. Bernard Tandler provided editorial assistance.

827 We thank Dr. Solomon Snyder for providing us with plasmids for recombinant
828 GAPDH expression. We thank Dr. Martin Jendrisak and the entire team of the
829 Gift of Hope Organ and Tissue Donor Network in Chicago for the human
830 pancreas tissues used in this study. We also thank Jing Wu, Xia Liu, Scott A.

831 Becka, Case Western Reserve University, for technical assistance. We thank
832 Ken Farabough for assistance with the manuscript preparation. We acknowledge
833 the Vector Biolabs (Philadelphia, USA) providing the adenovirus-mediated
834 shRNA for Cth knockdown experiment. This work was supported by NIH grants
835 R37-DK060596, R01-DK053307 (to MH), R01-HL58984 (to RB), R01-DK013499
836 (to ML) and NIH DK48280 (to PA), Canada Excellence Research Chair grant
837 CERC08 (to LD), and an American Heart Association grant (13SDG17070096 to
838 O.K.). The Orbitrap Elite instrument was purchased via an NIH shared instrument
839 grant 1S10RR031537-01.

840

841 **References**

- 842 Altaany, Z., Ju, Y., Yang, G., and Wang, R. (2014). The coordination of S-
843 sulfhydration, S-nitrosylation, and phosphorylation of endothelial nitric oxide
844 synthase by hydrogen sulfide. *Science signaling* 7, ra87.
- 845 Anastasiou, D., Pouligiannis, G., Asara, J.M., Boxer, M.B., Jiang, J.K., Shen, M.,
846 Bellinger, G., Sasaki, A.T., Locasale, J.W., Auld, D.S., *et al.* (2011). Inhibition of
847 pyruvate kinase M2 by reactive oxygen species contributes to cellular antioxidant
848 responses. *Science* 334, 1278-1283.
- 849 Berman, H.M., Westbrook, J., Feng, Z., Gilliland, G., Bhat, T.N., Weissig, H.,
850 Shindyalov, I.N., and Bourne, P.E. (2000). The Protein Data Bank. *Nucleic acids*
851 *research* 28, 235-242.
- 852 Dickhout, J.G., Carlisle, R.E., Jerome, D.E., Mohammed-Ali, Z., Jiang, H., Yang,
853 G., Mani, S., Garg, S.K., Banerjee, R., Kaufman, R.J., *et al.* (2012). Integrated
854 stress response modulates cellular redox state via induction of cystathionine
855 gamma-lyase: cross-talk between integrated stress response and thiol
856 metabolism. *The Journal of biological chemistry* 287, 7603-7614.
- 857 Finkel, T. (2012). Signal transduction by mitochondrial oxidants. *The Journal of*
858 *biological chemistry* 287, 4434-4440.
- 859 Forrester, M.T., Foster, M.W., Benhar, M., and Stamler, J.S. (2009). Detection of
860 protein S-nitrosylation with the biotin-switch technique. *Free radical biology &*
861 *medicine* 46, 119-126.
- 862 Gao, X.H., Zaffagnini, M., Bedhomme, M., Michelet, L., Cassier-Chauvat, C.,
863 Decottignies, P., and Lemaire, S.D. (2010). Biochemical characterization of
864 glutaredoxins from *Chlamydomonas reinhardtii*: kinetics and specificity in
865 deglutathionylation reactions. *FEBS letters* 584, 2242-2248.
- 866 Guan, B.J., Krokowski, D., Majumder, M., Schmotzer, C.L., Kimball, S.R.,
867 Merrick, W.C., Koromilas, A.E., and Hatzoglou, M. (2014). Translational control
868 during endoplasmic reticulum stress beyond phosphorylation of the translation
869 initiation factor eIF2alpha. *The Journal of biological chemistry* 289, 12593-12611.
- 870 Han, J., Back, S.H., Hur, J., Lin, Y.H., Gildersleeve, R., Shan, J., Yuan, C.L.,
871 Krokowski, D., Wang, S., Hatzoglou, M., *et al.* (2013). ER-stress-induced

872 transcriptional regulation increases protein synthesis leading to cell death. *Nature*
873 *cell biology* 15, 481-490.

874 Hara, M.R., Agrawal, N., Kim, S.F., Cascio, M.B., Fujimuro, M., Ozeki, Y.,
875 Takahashi, M., Cheah, J.H., Tankou, S.K., Hester, L.D., *et al.* (2005). S-
876 nitrosylated GAPDH initiates apoptotic cell death by nuclear translocation
877 following Siah1 binding. *Nature cell biology* 7, 665-674.

878 Harding, H.P., Zhang, Y., Zeng, H., Novoa, I., Lu, P.D., Calton, M., Sadri, N.,
879 Yun, C., Popko, B., Paules, R., *et al.* (2003). An integrated stress response
880 regulates amino acid metabolism and resistance to oxidative stress. *Molecular*
881 *cell* 11, 619-633.

882 Hetz, C. (2012). The unfolded protein response: controlling cell fate decisions
883 under ER stress and beyond. *Nature reviews. Molecular cell biology* 13, 89-102.

884 Hine, C., Harputlugil, E., Zhang, Y., Ruckenstuhl, C., Lee, B.C., Brace, L.,
885 Longchamp, A., Trevino-Villarreal, J.H., Mejia, P., Ozaki, C.K., *et al.* (2015).
886 Endogenous hydrogen sulfide production is essential for dietary restriction
887 benefits. *Cell* 160, 132-144.

888 Kabil, O., and Banerjee, R. (2010). Redox biochemistry of hydrogen sulfide. *The*
889 *Journal of biological chemistry* 285, 21903-21907.

890 Kabil, O., Vitvitsky, V., Xie, P., and Banerjee, R. (2011). The quantitative
891 significance of the transsulfuration enzymes for H₂S production in murine
892 tissues. *Antioxidants & redox signaling* 15, 363-372.

893 Kabsch, W., and Sander, C. (1983). Dictionary of protein secondary structure:
894 pattern recognition of hydrogen-bonded and geometrical features. *Biopolymers*
895 22, 2577-2637.

896 Kortemme, T., and Creighton, T.E. (1995). Ionisation of cysteine residues at the
897 termini of model alpha-helical peptides. Relevance to unusual thiol pK_a values in
898 proteins of the thioredoxin family. *Journal of molecular biology* 253, 799-812.

899 Krishnan, N., Fu, C., Pappin, D.J., and Tonks, N.K. (2011). H₂S-Induced
900 sulfhydration of the phosphatase PTP1B and its role in the endoplasmic
901 reticulum stress response. *Science signaling* 4, ra86.

902 Krokowski, D., Han, J., Saikia, M., Majumder, M., Yuan, C.L., Guan, B.J.,
903 Bevilacqua, E., Bussolati, O., Broer, S., Arvan, P., *et al.* (2013a). A Self-
904 Defeating Anabolic Program Leads to beta cell apoptosis in ER Stress-Induced
905 Diabetes via Regulation of Amino Acid Flux. *The Journal of biological chemistry*.
906 Krokowski, D., Han, J., Saikia, M., Majumder, M., Yuan, C.L., Guan, B.J.,
907 Bevilacqua, E., Bussolati, O., Broer, S., Arvan, P., *et al.* (2013b). A self-defeating
908 anabolic program leads to beta-cell apoptosis in endoplasmic reticulum stress-
909 induced diabetes via regulation of amino acid flux. *The Journal of biological*
910 *chemistry* 288, 17202-17213.

911 Marino, S.M., and Gladyshev, V.N. (2011). Redox biology: computational
912 approaches to the investigation of functional cysteine residues. *Antioxidants &*
913 *redox signaling* 15, 135-146.

914 Mishanina, T.V., Libiad, M., and Banerjee, R. (2015). Biogenesis of reactive
915 sulfur species for signaling by hydrogen sulfide oxidation pathways. *Nature*
916 *chemical biology* 11, 457-464.

917 Morisse, S., Zaffagnini, M., Gao, X.H., Lemaire, S.D., and Marchand, C.H.
918 (2014). Insight into protein S-nitrosylation in *Chlamydomonas reinhardtii*.
919 *Antioxidants & redox signaling* 21, 1271-1284.

920 Mustafa, A.K., Gadalla, M.M., Sen, N., Kim, S., Mu, W., Gazi, S.K., Barrow, R.K.,
921 Yang, G., Wang, R., and Snyder, S.H. (2009). H₂S signals through protein S-
922 sulfhydration. *Science signaling* 2, ra72.

923 Nishida, M., Sawa, T., Kitajima, N., Ono, K., Inoue, H., Ihara, H., Motohashi, H.,
924 Yamamoto, M., Suematsu, M., Kurose, H., *et al.* (2012). Hydrogen sulfide anion
925 regulates redox signaling via electrophile sulfhydration. *Nature chemical biology*
926 8, 714-724.

927 Niu, W.N., Yadav, P.K., Adamec, J., and Banerjee, R. (2015). S-glutathionylation
928 enhances human cystathionine beta-synthase activity under oxidative stress
929 conditions. *Antioxidants & redox signaling* 22, 350-361.

930 O'Shea, J.P., Chou, M.F., Quader, S.A., Ryan, J.K., Church, G.M., and Schwartz,
931 D. (2013). pLogo: a probabilistic approach to visualizing sequence motifs. *Nature*
932 *methods* 10, 1211-1212.

933 Pan, J., and Carroll, K.S. (2013). Persulfide reactivity in the detection of protein
934 s-sulfhydration. *ACS chemical biology* 8, 1110-1116.

935 Paul, B.D., and Snyder, S.H. (2012). H₂S signalling through protein
936 sulfhydration and beyond. *Nature reviews. Molecular cell biology* 13, 499-507.

937 Saikia, M., Jobava, R., Parisien, M., Putnam, A., Krokowski, D., Gao, X.H., Guan,
938 B.J., Yuan, Y., Jankowsky, E., Feng, Z., *et al.* (2014). Angiogenin-cleaved tRNA
939 halves interact with cytochrome c, protecting cells from apoptosis during osmotic
940 stress. *Molecular and cellular biology* 34, 2450-2463.

941 Sen, N., Paul, B.D., Gadalla, M.M., Mustafa, A.K., Sen, T., Xu, R., Kim, S., and
942 Snyder, S.H. (2012). Hydrogen sulfide-linked sulfhydration of NF-kappaB
943 mediates its antiapoptotic actions. *Molecular cell* 45, 13-24.

944 Szabo, C., Coletta, C., Chao, C., Modis, K., Szczesny, B., Papapetropoulos, A.,
945 and Hellmich, M.R. (2013). Tumor-derived hydrogen sulfide, produced by
946 cystathionine-beta-synthase, stimulates bioenergetics, cell proliferation, and
947 angiogenesis in colon cancer. *Proceedings of the National Academy of Sciences*
948 *of the United States of America* 110, 12474-12479.

949 Tabas, I., and Ron, D. (2011). Integrating the mechanisms of apoptosis induced
950 by endoplasmic reticulum stress. *Nature cell biology* 13, 184-190.

951 Touw, W.G., Baakman, C., Black, J., te Beek, T.A., Krieger, E., Joosten, R.P.,
952 and Vriend, G. (2015). A series of PDB-related databanks for everyday needs.
953 *Nucleic acids research* 43, D364-368.

954 van Dijk, T.H., van der Sluijs, F.H., Wiegman, C.H., Baller, J.F., Gustafson, L.A.,
955 Burger, H.J., Herling, A.W., Kuipers, F., Meijer, A.J., and Reijngoud, D.J. (2001).
956 Acute inhibition of hepatic glucose-6-phosphatase does not affect
957 gluconeogenesis but directs gluconeogenic flux toward glycogen in fasted rats. A
958 pharmacological study with the chlorogenic acid derivative S4048. *The Journal of*
959 *biological chemistry* 276, 25727-25735.

960 Vander Heiden, M.G., Cantley, L.C., and Thompson, C.B. (2009). Understanding
961 the Warburg effect: the metabolic requirements of cell proliferation. *Science* 324,
962 1029-1033.

963 Vishnu, N., Jadoon Khan, M., Karsten, F., Groschner, L.N., Waldeck-Weiermair,
964 M., Rost, R., Hallstrom, S., Imamura, H., Graier, W.F., and Malli, R. (2014). ATP
965 increases within the lumen of the endoplasmic reticulum upon intracellular Ca²⁺
966 release. *Molecular biology of the cell* 25, 368-379.

967 Wallace, J.L., and Wang, R. (2015). Hydrogen sulfide-based therapeutics:
968 exploiting a unique but ubiquitous gasotransmitter. *Nature reviews. Drug*
969 *discovery* 14, 329-345.

970 Walter, P., and Ron, D. (2011). The unfolded protein response: from stress
971 pathway to homeostatic regulation. *Science* 334, 1081-1086.

972 Weerapana, E., Wang, C., Simon, G.M., Richter, F., Khare, S., Dillon, M.B.,
973 Bachovchin, D.A., Mowen, K., Baker, D., and Cravatt, B.F. (2010). Quantitative
974 reactivity profiling predicts functional cysteines in proteomes. *Nature* 468, 790-
975 795.

976 Xue, Y., Liu, Z., Gao, X., Jin, C., Wen, L., Yao, X., and Ren, J. (2010). GPS-
977 SNO: computational prediction of protein S-nitrosylation sites with a modified
978 GPS algorithm. *PloS one* 5, e11290.

979 Yang, L., Kombu, R.S., Kasumov, T., Zhu, S.H., Cendrowski, A.V., David, F.,
980 Anderson, V.E., Kelleher, J.K., and Brunengraber, H. (2008). Metabolomic and
981 mass isotopomer analysis of liver gluconeogenesis and citric acid cycle. I.
982 Interrelation between gluconeogenesis and cataplerosis; formation of
983 methoxamates from aminooxyacetate and ketoacids. *The Journal of biological*
984 *chemistry* 283, 21978-21987.

985

986

987 **Figure titles and legends**

988 **Figure 1. ER stress induces protein sulfhydration, a reversible cysteine-**

989 **based post-translational modification.** (A) Schematic overview of protein

990 sulfhydration, which requires synthesis of H₂S and low ROS levels. Pancreatic β

991 cells (MIN6) were treated with thapsigargin (Tg) for the indicated times, and the

992 cellular levels of ROS (B), total levels of GSH and GSH/GSSG ratios (C) and H₂S

993 levels (E) were evaluated. (D) RT-qPCR analysis of the mRNA levels for the H₂S-

994 producing enzyme CTH and the cystine/glutamate exchanger Slc7a11 in MIN6

995 cells treated with Tg or pancreatic islets as indicated. (F) Evaluation of GAPDH

996 activity in cell extracts from MIN6 cells treated with Tg at the indicated times

997 (top), and GAPDH protein levels by Western blot analysis (bottom). (G). Time-

998 dependent measurements of human recombinant GAPDH activities after

999 exposure to H₂O₂ (50 μM, □□□e) or H₂O₂ together with the H₂S donor, NaHS

1000 (50 μM, red). □H) In vitro evaluation of the reversal of the inhibitory effect of

1001 glutathionylation on the activity of recombinant GAPDH treated for 15 min with

1002 either NaHS (20 mM), DTT (20 mM) or NaCl (20 mM). (I). Evaluation of GAPDH

1003 activities in MIN6 cell extracts either untreated or treated with Tg (18 h) with or

1004 without the Cth inhibitor, PAG (3 mM) (top). PAG was included for the last 3.5 h

1005 of Tg-treatment. GAPDH protein levels were evaluated by Western blotting

1006 (bottom). All quantifications are presented as mean ± S.E.M. of three

1007 independent experiments.

1008

1009 **Figure 2. ATF4-mediated transcriptional reprogramming during ER stress**
1010 **increases expression of a gene cohort involved in H₂S synthesis and**
1011 **protein sulfhydration. (A)** Schematic representation of the ATF4-induced
1012 cohort of genes leading to sulfhydration of proteins during ER stress. **(B)**
1013 Evaluation of intracellular H₂S levels (top) or ATF4 and Cth protein levels
1014 (bottom) in MIN6 cells infected with either control shRNA or shRNA against
1015 ATF4. Cells were untreated or treated with Tg for 18 h. **(C)** Western blot analysis
1016 for the indicated proteins in MIN6 cells infected (for 48 h) with either adenovirus
1017 mediated lacZ-expression as control, or ATF4-expression, at increasing viral
1018 particle concentrations. MIN6 cells infected with either control adenovirus or
1019 ATF4-expressing adenovirus were used to measure **(D)** H₂S levels **(E)** GAPDH
1020 relative activities, **(F)** GSH levels and **(G)** Glutamate (Glu) uptake by the
1021 cystine/glutamate exchanger. **(H)** Schematic representation of the novel Biotin-
1022 Thiol-Assay (BTA), an experimental approach for the identification of
1023 sulfhydrated proteins in cell extracts. Highly reactive cysteine residues or
1024 sulfhydrated cysteine residues in proteins under native conditions were alkylated
1025 with low concentrations of maleimide-PEG2-biotin (NM-Biotin). Subsequent
1026 avidin column purification and elution with DTT, which cleaved the disulfide
1027 bonds, leaving the biotin tag bound to the column, produced an eluate that was
1028 further analyzed either by western blotting or coupled with LC-MS/MS. **(I)**
1029 Identification via the BTA of sulfhydrated GAPDH in MIN6 cell extracts from Tg-
1030 treated cells in the presence or absence of ATF4. **(J)** Identification of
1031 sulfhydrated GAPDH in MIN6 cells overexpressing ATF4. **(K)** Determination of

1032 the effect of PAG on sulfhydrated GAPDH levels in MIN6 cells overexpressing
1033 ATF4 in the presence or absence of PAG.
1034

1035 **Figure 3. Quantitative and pathway analysis of sulfhydrated peptides in**
1036 **MIN6 cells overexpressing the transcription factor ATF4. (A)** Schematic
1037 representation of the BTA experimental approach combined with alkylation of
1038 free SH groups by either the stable isotope-labeled (D₅, heavy) or normal (H₅,
1039 light) maleimide. The relative levels of H₅ and D₅ labeled peptides were
1040 quantified by the LC-MS/MS method. **(B)** Distribution of peptides containing
1041 sulfhydrated cysteine residues relative to their H/L ratios as determined by the
1042 BTA analysis of cell extracts isolated from MIN6 cells overexpressing ATF4
1043 (indicated in **A**). Values of H/L ratios are plotted against the number of identified
1044 peptides. The red line marks the H/L ratio >2, consisting of cysteine-containing
1045 peptides in proteins that exhibited higher reactivity with H₂S under ATF4
1046 overexpression. The black dots show redox sensitive cysteine peptides, which
1047 are common between the ones found in the RedoxDB database, and by the BTA
1048 assay. **(C)** Pie chart illustrating the percentage of cysteine-containing peptides
1049 (from **A**) that belong to known functional domains of proteins in the Uniprot
1050 database. **(D)** Heat map of H/L values obtained from experimental data in **(A)**,
1051 illustrating the profound differences in the reactivity with H₂S of cysteine residues
1052 in different proteins. **(E)** Gene ontology biological pathways for peptides with H/L
1053 ratio >2. H/L values were obtained from the experimental data in **(A)**.
1054

1055 **Figure 4. H₂S synthesis during ER stress modulates metabolism in MIN6**
1056 **cells. (A)** Measurement of ¹³C-glucose flux in metabolites, expressed as the
1057 molar percent enrichment [(ratio of labeled/sum (labeled + unlabeled) x 100%)],
1058 in MIN6 cells treated with Tg for 18 h or after addition of PAG for the last 3.5 h of
1059 Tg treatment. [U-¹³C]-glucose replaced glucose in the media for the last 3.5 h of
1060 treatments. **(B)** Evaluation of the concentration of metabolites and amino acids in
1061 the same samples described in **(A)**. All quantifications are presented as mean ±
1062 S.E.M. of technical duplicates and are represented four independent
1063 experiments. **(C)** Schematic representation of the major findings on metabolic
1064 flux from glucose during chronic ER stress. Chronic ER stress increased
1065 glycolytic flux and decreased forward TCA flux. Inhibition of CTH by PAG
1066 reversed the observed changes in glucose flux during ER stress.
1067

1068 **Figure 1-figure supplement 1.**

1069 ER stress induces the levels of the H₂S-producing enzyme CTH but not CBS.
1070 Western blot analysis for the indicated proteins, of cell extracts isolated from Tg
1071 treated MIN6 cells for the indicated times.

1072

1073 **Figure 1-figure supplement 2.**

1074 **Regulation of gene expression in MIN6 cells, human and mouse islets in**
1075 **response to ER stress.** MIN6 cells (A) and human islets (B) were treated with
1076 Tg for the indicated times. Islets were isolated from WT and heterozygous Akita
1077 *Ins2*^{c96y} six-week old mice (C). RNA was isolated from cells and islets and was
1078 tested by RT-qPCR for expression of the indicated genes.

1079

1080 **Figure 1-figure supplement 3.**

1081 **Activation of the Integrated Stress Response leads to increased expression**
1082 **of CTH in wild type mouse islets treated with Tg.** Western blot analysis for the
1083 indicated proteins of cell extracts isolated from Tg treated islets for 24 h.

1084

1085 **Figure1-figure supplement 4**

1086 **Glutamate uptake in MIN6 cells treated with Tg at the indicated times.**

1087

1088 **Figure 1-figure supplement 5.**

1089 **Analysis of S-glutathionylated GAPDH by LC-MS/MS.** Recombinant GAPDH
1090 (20 µg) was treated with GSSG (5 mM) for 45 min, then incubated with 50 mM of

1091 NEM. The sample was resolved by SDS-PAGE electrophoresis and analyzed by
1092 LC-MS/MS. Tandem mass spectrum of the active site peptide
1093 IISNASCTTNCLAPLAK of the protein with glutathionylated Cys¹⁵⁰, and Cys¹⁵⁴
1094 alkylated with NEM. Comparison with the same peptide both NEM alkylation,
1095 there are no mass changes of y series ions from y4 to y10 and b series ions from
1096 b2 to b4, but a mass shift from y11 to y16, and b8, b9 ions, which strongly
1097 suggests the modification at Cys¹⁵⁰. @ represents the neutral loss of -129Da
1098 from a glutathione adduct.

1099

1100 **Figure 2-figure supplement 1.**

1101 Expression of genes in MIN6 cells overexpressing the transcription factor ATF4.
1102 RT-qPCR analysis of RNA isolated from cells infected with control adenovirus (-)
1103 or ATF4-expressing adenovirus (+) for 48 h, for the indicated genes. The results
1104 are shown as the average of three independent determinations.

1105

1106 **Figure 2-figure supplement 2.**

1107 **Schematic representation of the predicted proteins in the eluate of the BTA**
1108 **approach as a consequence of increasing concentrations of biotin**
1109 **conjugated maleimide (NM-biotin, red).** At low concentration (top), the high
1110 reactive -SH groups (orange) including unmodified and sulfhydrated cysteines
1111 are discriminated for alkylation, leading to elution of sulfhydrated proteins from
1112 the avidin column by DTT. At the high concentration (bottom), all -SH groups in

1113 cysteines are labeled, leading to the proteins permanently bound to the beads
1114 and unable to be eluted by DTT.

1115

1116 **Figure 2-figure supplement 3.**

1117 Increasing concentrations of NM-biotin in the BTA of cell extracts isolated from
1118 Tg treated for 18 h MIN6 cells, inhibit the elution of sulfhydrated proteins. Eluted
1119 proteins were analysed by SDS-PAGE and stained by Coomassie blue. Western
1120 blot analysis for tubulin, of equal amount of MIN6 cell extracts before binding to
1121 the avidin column.

1122

1123 **Figure 2-figure supplement 4.**

1124 **H₂S covalently modifies proteins via sulfhydration of cysteine residues. (A)**

1125 Mouse liver lysates were subjected to NM-biotin, then divided in 8 equal
1126 fractions, were bound on avidin columns and eluted by the addition of the
1127 indicated concentrations of DTT. The eluates were analysed by SDS-PAGE
1128 electrophoresis and stained by Coomassie blue. **(B)** Lysates from MIN6 cells
1129 treated with Tg for 18 h, were pretreated with or without 20 mM DTT for 20 min,
1130 and after passing through a NAP-5 gel filtration column, were subjected to the
1131 BTA assay followed by SDS-PAGE electrophoresis and silver staining of the
1132 gels. Equal amount of extracts before loading on the avidin columns were
1133 analysed by western blotting for tubulin. DTT treatment of extracts before the
1134 avidin column, reversed global protein sulfhydration, implying a covalent
1135 cysteine-based modification.

1136

1137 **Figure 2-figure supplement 5.**

1138 **Assessment of the specificity of BTA to identify reactive -S-SH groups of**
1139 **proteins via the use of recombinant GAPDH. (A)** The purity of human
1140 recombinant GAPDH was evaluated by SDS-PAGE electrophoresis and was
1141 stained by Coomassie blue. *- indicates GST-tagged GAPDH. **(B)** Recombinant
1142 GAPDH (100 µg) was incubated for 45 min with 50 µM NaCl, as the control, H₂O₂
1143 (mediating oxidation of cysteines) or NaHS (mediating sulfhydrylation of
1144 cysteines). Following desalting, samples were subjected to the BTA assay.
1145 Eluates were analyzed by Western blotting for GAPDH. Extracts from samples
1146 before loading to the avidin column were also analyzed by Western blotting for
1147 GAPDH (input).

1148

1149 **Figure 2-figure supplement 6.**

1150 **Assessment of GAPDH sulfhydrylation by the red maleimide assay.**
1151 Recombinant GAPDH (20 µg) was exposed to NaHS (50 µM), or NaCl (50 µM)
1152 as the control, for 45 min. The levels of sulfhydrylated GAPDH were evaluated with
1153 the red maleimide assay and measured by the decreasing fluorescence intensity
1154 after β-mercaptoethanol (β-ME) treatment.

1155

1156 **Figure 2-figure supplement 7.**

1157 **BTA identifies sulfhydrylation of GAPDH at the catalytic cysteine, Cys¹⁵⁰.** (A)
1158 Both wild type (WT) and Cys¹⁵⁰Ser recombinant GAPDH mutant (100 µg) were

1159 incubated with 50 μ M each, NaHS, H₂O₂ or NaCl (as the control), for 45 min.
1160 After desalting, samples were subjected to the BTA assay. Eluates were
1161 analyzed by Western blot analysis for GAPDH. Sulfhydrylation was observed only
1162 for the WT GAPDH. **(B)** Wild type recombinant GAPDH (20 μ g) was pretreated
1163 with DTT (20 mM) for 45 min following desalting. The protein was subsequently
1164 incubated with or without NaHS (50 μ M) for 45 min, followed with treatment with
1165 NEM (50 mM). The latter treatment is expected to block all free -SH groups. The
1166 samples were resolved by SDS-PAGE electrophoresis followed by LC-MS/MS
1167 analysis. The NaHS-treated GAPDH showed a mass shift of Cys¹⁵⁰
1168 corresponding to the sulfinic acid due to sulfhydrylation (bottom). The oxidation of
1169 the S-SH group of Cys¹⁵⁰ to sulfinic acid is expected due to its high reactivity
1170 when exposed to O₂ under the aerobic conditions of the experiment.

1171

1172 **Figure 2-figure supplement 8.**

1173 **The BTA assay shows that Tg-induced ER stress in MIN6 cells promotes**
1174 **global protein sulfhydrylation.** **(A)** The BTA assay was performed to detect
1175 protein sulfhydrylation in extracts from MIN6 cells treated with Tg for 18 h. **(B)**
1176 Western blot analysis confirmed that GAPDH was sulfhydrated in MIN6 cells
1177 during Tg treatment. **(C)** GAPDH activity in cell extracts from untreated or Tg-
1178 treated MIN6 cells for 18 h. **(D)** LC-MS/MS of a subset of the sulfhydrated
1179 proteins in **(A)**, including GAPDH, actin and β -tubulin (Mustafa et al., 2009).

1180

1181 **Figure 2-figure supplement 9.**

1182 **LC-MS/MS spectrum of H₂S-modified peptides purified by the BTA**
1183 **technique from MIN6 cells treated with Tg for 18 h.**

1184

1185 **Figure 2-figure supplement 10.**

1186 **Western blot analysis of eluates from the BTA of sulfhydrated GAPDH and**
1187 **PHGDH in MIN6 cells treated with Tg in a time-dependent manner.**

1188

1189 **Figure 2-figure supplement 11.**

1190 Western blot analysis for CTH protein levels from MIN6 cells infected with either
1191 adenovirus-mediated expression of GFP as control, or shRNA against the CTH
1192 mRNA in a dose- **(A)** and time- **(B)** dependent manner. **(C)** Western blot analysis
1193 of the indicated proteins from cell extracts before applying to the column (input)
1194 or after the column (eluate). The effects of CTH knockdown by shRNA on
1195 sulfhydrated GAPDH and PHGDH levels in MIN6 cells treated with or without Tg
1196 for 18h, is shown.

1197

1198 **Figure 3-figure supplement 1.**

1199 **Sulfhydrated cysteine-containing peptides are enriched in functional**
1200 **residues.** Distribution of peptides containing sulfhydrated cysteines relative to
1201 their H/L ratios with functional annotations from the Uniprot database where
1202 active sites (ACT_SITE), binding sites (BINDING), calcium binding sites
1203 (CA_BIND), disulfide bonds (DISULFID), DNA binding sites (DNA_BIND),
1204 specific domains (DOMAIN), metal binding sites (METAL), modified residues

1205 (MOD_RES), motifs with biological activity (MOTIF), nucleotide binding sites
1206 (NP_BIND) and zinc finger domains (ZN_FING) are shown as black dots.

1207

1208 **Figure 3-figure supplement 2.**

1209 **Sulfhydrated proteins are potential targets for nitrosylation.** A total of 827
1210 H₂S-modified and pair-labeled peptides were scored for their nitrosylation
1211 potential via the use of the GPS-SNO algorithm. We identified 303 peptides with
1212 predicted S-nitrosylation sites. Among them, only 5 peptides (red dots) had an
1213 H/L ratio below 2 (1.5% of the scored peptides for S-nitrosylation).

1214

1215 **Figure 3-figure supplement 3.**

1216 **Quantitative profiling of proteins containing cysteines with different**
1217 **reactivity to H₂S from ATF4 overexpressing MIN6 cells.** MS1 profiles for
1218 multiple cysteine-containing peptides from GDI1, PHGDH, VCP and LAP3, only
1219 one of which exhibits the highest reactivity with H₂S, as shown by the H/L ratios.

1220

1221 **Figure 3-figure supplement 4.**

1222 **(A-B)** Sulfhydrated peptides do not reveal a consensus sequence motif, but the
1223 modified cysteine residue is significantly accessible and preferentially positioned
1224 at the N-terminal of alpha helix. **(A)** A total of 739 pair-labeled peptide sequences
1225 were used to show that no primary sequence motif could be detected using the
1226 pLogo program. **(B)** A total of 333 peptides with H/L ratios over 2-fold showed
1227 significant enrichment for Arg residue found next to the modified cysteine. **(C-D)**

1228 the surface accessibility and secondary structure of the modified cysteine
1229 residues in peptides were annotated by comparing those peptides with H/L ratios
1230 greater than 2-fold and proteins with known structures in the PDB database (172
1231 protein structures were employed). In the secondary structure motif, H= alpha
1232 helix; G=3₁₀-helix; E=beta sheet; T= helix turn; S=bend (high curvature).

1233

1234 **Figure 3-figure supplement 5.**

1235 **Gene ontology biological pathways enriched among all pair-labeled**
1236 **peptides in ATF4 overexpressed MIN6 cells.** 739 pair-labeled cysteine-
1237 containing peptides were subjected to a pathway analysis carried by the Davide
1238 and IPA programs (**A, B**). (**C-D**) the proteins associated with the H/L greater
1239 than 2-fold were selected and subjected for both pathway annotation
1240 calculations. Top 5 pathways are shown with their statistical significance
1241 (Bonferroni correction for N=17 tests).

1242

1243 **Figure 3-figure supplement 6.**

1244 **MS analysis of the full proteome from MIN6 cells treated with Tg for 18h.**

1245 **Cell extracts were resolved by reducing SDS-PAGE and stained with**

1246 **Coomassie blue.** The entire gel lane was cut into 11 fractions for in-gel

1247 digestions. The peptides from each fraction were combined as indicated and

1248 submitted for LC-MS/MS analysis. A total of 2,244 proteins were quantified by

1249 label-free, semi-quantitative MS approaches.

1250

1251 **Figure 3-supplement figure 7.**

1252 **Protein sulfhydration does not correlate with their protein abundance.** The

1253 relative abundance of the proteins in the full proteome was determined based on

1254 the peptide spectral counts, which were corrected by normalizing to both the total

1255 number of spectra and the length of the protein, and this value was expressed as

1256 normal spectra abundance factor (NSAF). A comparison of the full protein

1257 abundance and sulfhydrome from Tg-treated (**A**), or ATF4 overexpressing MIN6

1258 (**B**). (**C**) A comparison of sulfhydrated protein datasets for the full proteome

1259 reveals that a large fraction of medium abundant proteins are mainly targeted by

1260 H₂S. (**D**) A comparison of sulfhydrated proteins with H/L ratios greater than 2-fold

1261 and the full proteome.

1262

1263 **Figure 4-figure supplement 1.**

1264 **ATF4 -overexpressing MIN6 cells exhibit significantly high glycolytic rates.**

1265 The rates of extracellular acidification (ECAR) were determined by using the

1266 Seahorse analyzer from ATF4 expressed MIN6 cells, or GFP as the control after
1267 48h of adenovirus infection. ECAR was normalized to cell numbers. The results
1268 are shown as a mean of four independent determinations.

1269

1270 **Figure 4-figure supplement 2.**

1271 **Pharmacological inhibition of CTH activity represses PKM2 activation in**
1272 **ATF4 overexpressed MIN6 cells.** Determination of the effect of PAG on the
1273 activity of PKM2 in MIN6 cells infected with either GFP as the control, or ATF4
1274 adenovirus for 48h. The activities are shown as a mean of four independent
1275 determinations.

1276

1277 **Figure 4-figure supplement 3.**

1278 **PKM2 activation depends on CTH activity during ER stress in MIN6**
1279 **cells.** (A) ER stress does not affect PKM2 protein levels. MIN6 cells were
1280 incubated with Tg at the indicated times. The protein expression was evaluated
1281 by Western blot analysis. (B) Western blot analysis of the expression of PKM2 in
1282 mouse islets. (C) Time-dependent increase of PKM2 activity in MIN6 cells treated
1283 with Tg at the indicated times. (D) Determination of the effect of PAG on the
1284 activity of PKM2 in MIN6 cells treated with Tg in the presence or absence of PAG
1285 (top) and on protein levels evaluated by Western blot analysis (bottom). For
1286 panels C and D the results are shown as a mean of four independent
1287 determinations.

1288 **Supplementary File 1. Metabolite flux and relative concentrations of**
1289 **metabolites from control (CON) and Tg-treated MIN6 cells for 18 h.** PAG was
1290 added for the last 3.5 h of Tg-treatment in the indicated experimental samples.
1291 **Notes:** the reported serine M+2 labeling reflects the 2 carbon atoms in the GC-
1292 MS fragment ion that was quantitated, and is expected to be predominantly
1293 derived from fully-labeled (M+3) serine.

1294

1295 **Figure 2-source data 1**

1296 Sulfhydrated proteins from MIN6 cells treated with Tg for 18h

1297

1298 **Figure 3-source data 1**

1299 Sulfhydrated proteins from ATF4 overexpressed MIN6 cells

1300

1301 **Figure 3- source data 2**

1302 Relative abundance of proteins in MIN6 cells treated with Tg for 18h

1303

1304

1305

1306

1307

1308

1309 **Primers used for RT-qPCR**

1310 **Mouse**

1311

1312 *Cbs* 5' CCTATGGTCAGAATCAACAAGAT
1313 5' TGATAGTGTCTCCAGGCTTCAA
1314
1315 *Cth* 5' GGGATGGCGGTGGCTCGTTT
1316 5' AGCCCGAGCACTGGCGTTTG
1317
1318 *Chop* 5' CAGGGTCAAGAGTAGTGAAGGT
1319 5' CTGGAAGCCTGGTATGAGGAT
1320
1321 *Ero1a* 5' CCTGGACGACTGTACCTGTG
1322 5' CAGAATGGCAGGGTTTGACG
1323
1324 *Gadd34* 5' TACCCCTGTCTCTGGTAACCT
1325 5' TGGCTTTGCATTGTACTIONCATCA
1326
1327 *Gapdh* 5' CGCCTGGAGAAACCTGCCAAGTATG
1328 5' GGTGGAAGAATGGGAGTTGCTGTTG
1329
1330 *Slc7a5* 5' CTGCTACAGCGTAAAGGC
1331 5' AACACAATGTTCCCCACGTC
1332
1333 *Slc7a11* 5' TGTCCACAAGCACACTCCTC
1334 5' CTGCCAGCCCCATAAAAAGC

1335
1336 **Human**
1337
1338 *β -actin* 5' TCCCTGGAGAAGAGCTACGA
1339 5' AGCACTGTGTTGGCGTACAG
1340
1341 *CTH* 5' GACTCTACATGTCCGAATGG
1342 5' AACCTGTACACTGACGCTTCA
1343
1344 *ERO1 α* 5' GCCCGTTTTATGCTTGATGT
1345 5' AACTGGGTATGGTGGCAGAC
1346
1347 *GADD34* 5' CGACTGCAAAGGCGGC
1348 5' CAGGAAATGGACAGTGACCTTCT
1349
1350 *MST* 5' CCACCAGTGGCTTAGACAGG
1351 5' CCGAGACGGCATTGAACCT
1352
1353 *SLC7A5* 5' ATCGGGAAGGGTGATGTGTC
1354 5'CAGGGGCAGGTTTCTGTAGG
1355
1356 *SLC7A11* 5' TGTGGGCATAACTGTAGTGATGG
1357 5' GCGTAATACTTGAATCTCTTCCTG

1358

1359

1360

1361

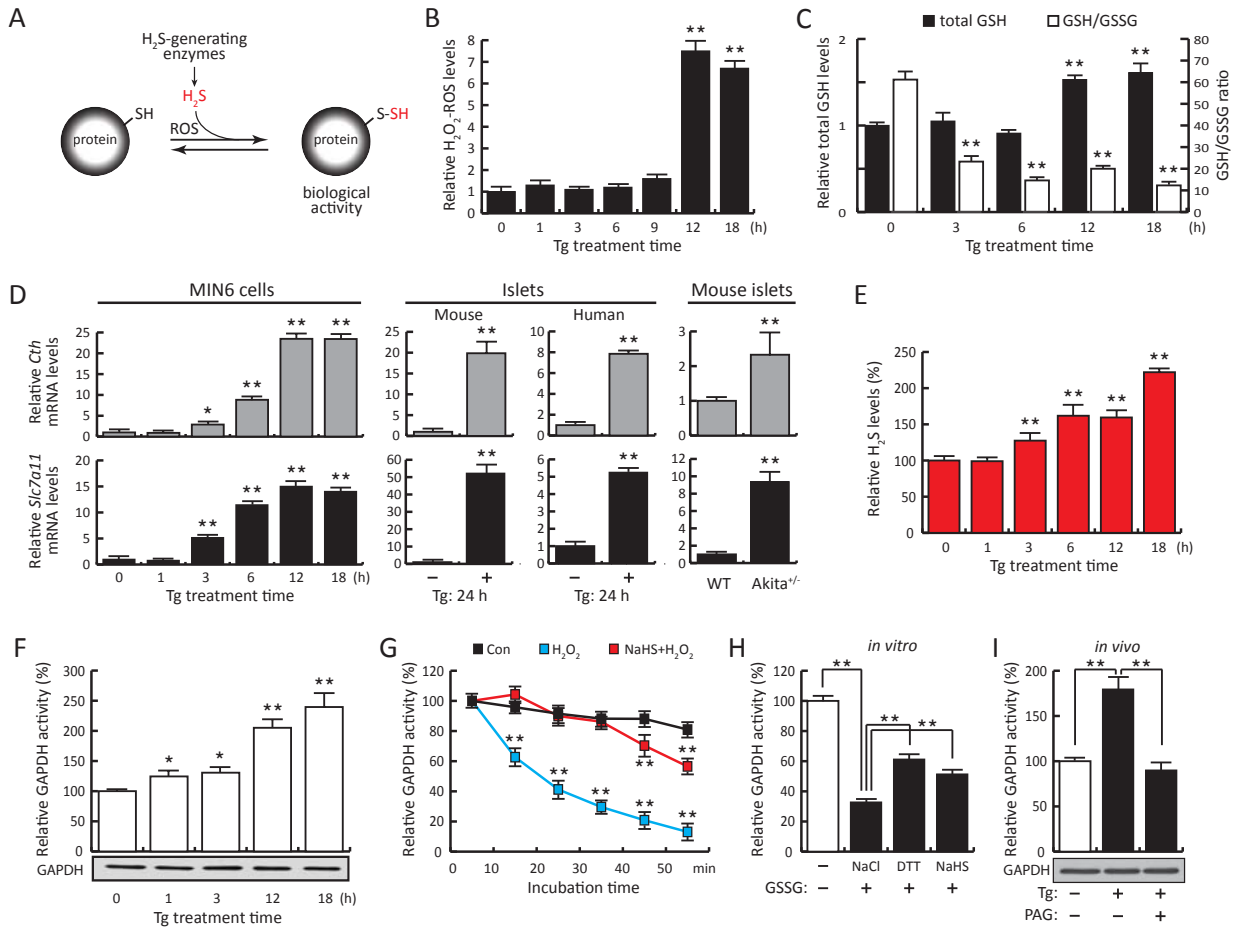


Figure 1.

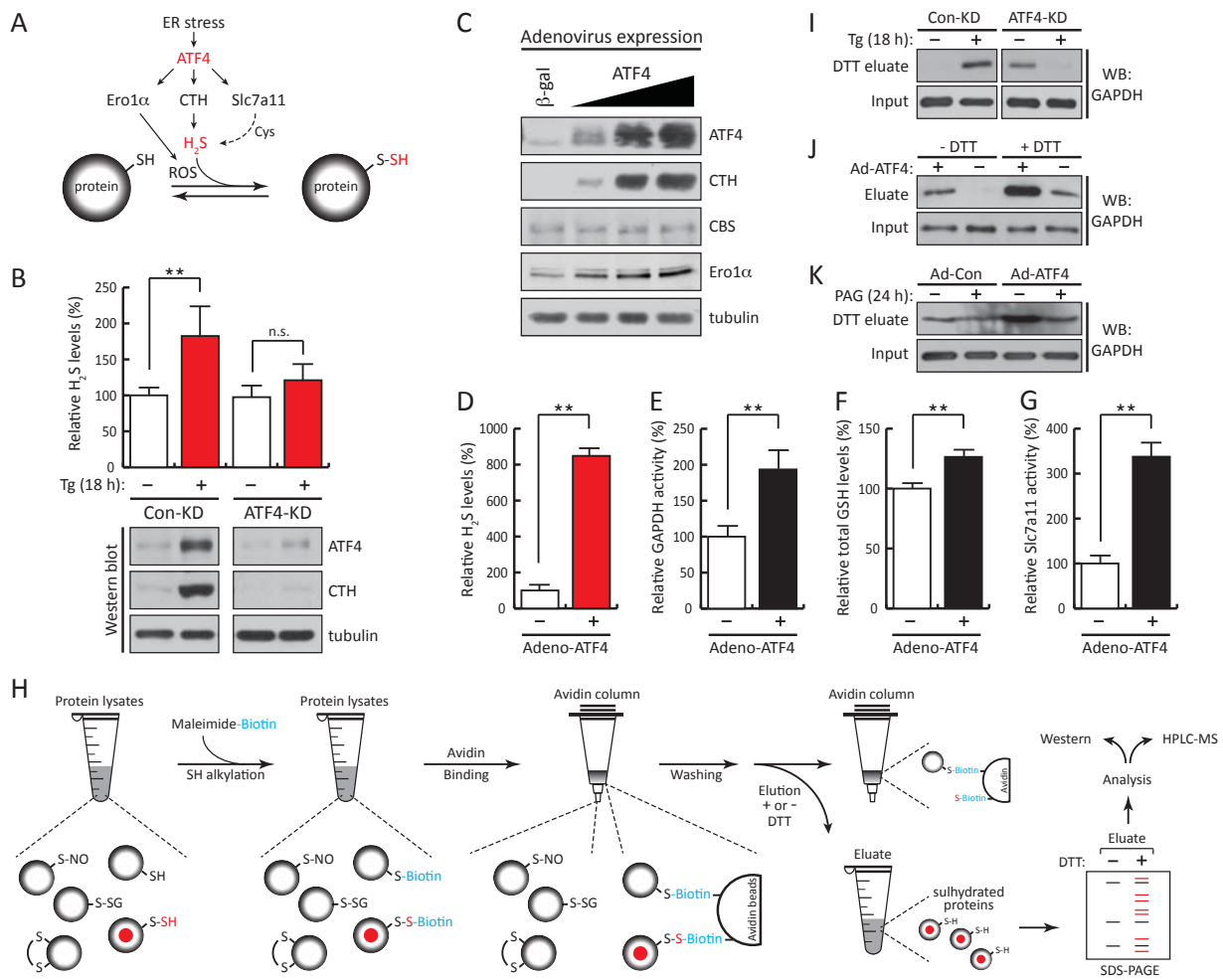


Figure 2.

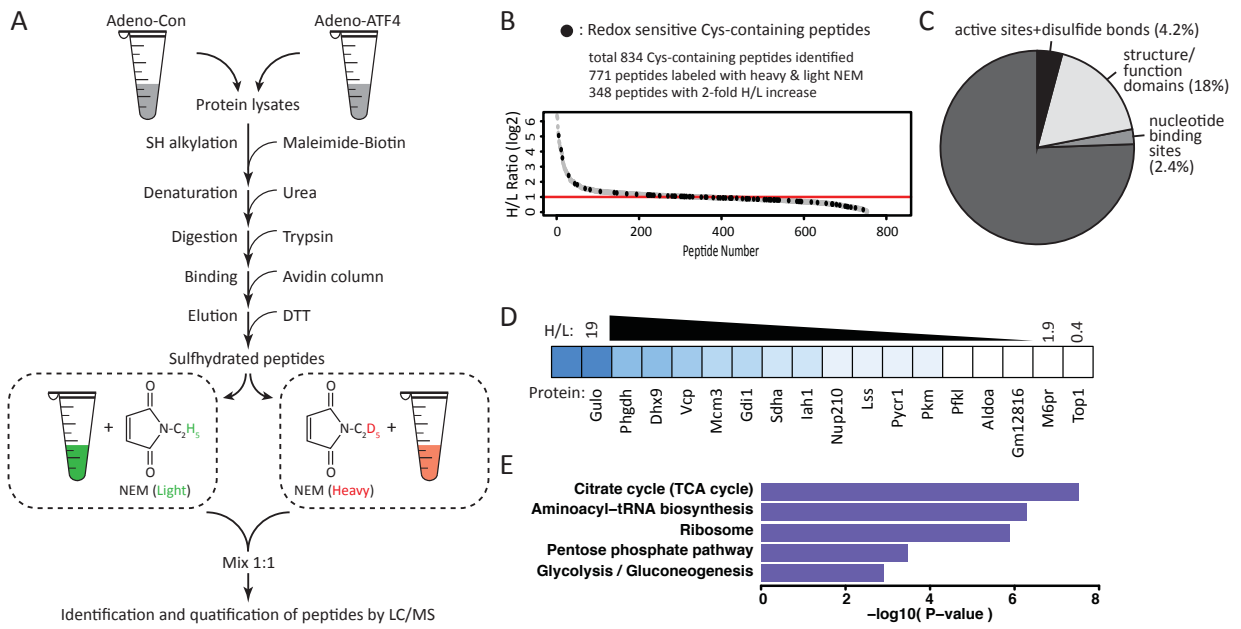
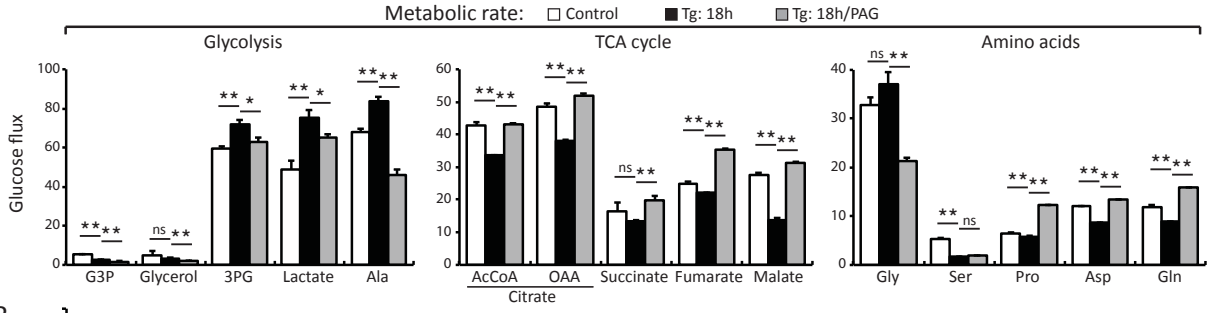


Figure 3.

A



B

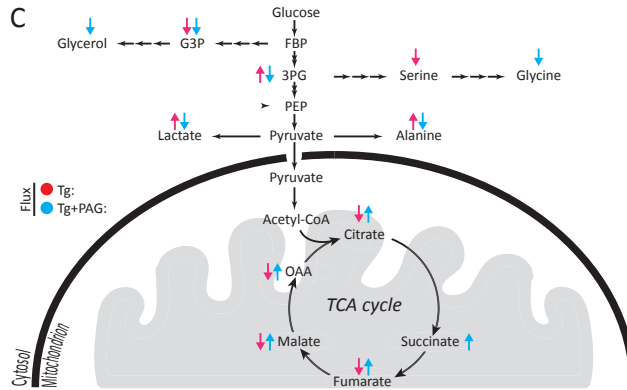
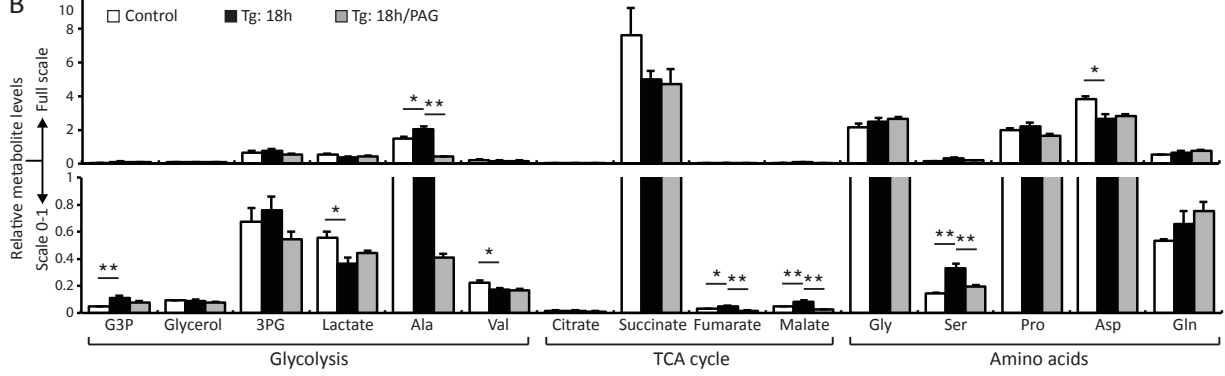


Figure 4.